NACA

RESEARCH MEMORANDUM

EXPERIMENTAL INVESTIGATION OF THE EFFECTS OF VISCOSITY

ON THE DRAG OF BODIES OF REVOLUTION

AT A MACH NUMBER OF 1.5

By

Dean R. Chapman and Edward W. Perkins

Ames Aeronautical Laboratory
Moffett Field, Calif.

NATIONAL ADVISORY COMMITTEE
FOR AERONAUTICS

WASHINGTON

April 3, 1947

NACA RM No. A7A31a
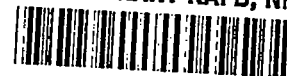
NATIONAL ADVISORY COMMITTEE FOR AERONAUTICS

RESEARCH MEMORANDUM

EXPERIMENTAL INVESTIGATION OF THE EFFECTS OF VISCOSITY

ON THE DRAG OF BODIES OF REVOLUTION

AT A MACH NUMBER OF 1.5

By Dean R. Chapman and Edward W. Perkins

SUMMARY

Tests were conducted to determine the effects of viscosity on the drag and base pressure characteristics of various bodies of revolution at a Mach number of 1.5. The models were tested both with smooth surfaces and with roughness added to evaluate the effects of Reynolds number for both laminar and turbulent boundary layers. The principal geometric variables investigated were afterbody shape and length-diameter ratio. For most models, force tests and base pressure measurements were made over a range of Reynolds numbers, based on model length, from 0.6 million to 5.0 millions. Schlieren photographs were used to analyze the effects of viscosity on flow separation and shock-wave configuration near the base and to verify the condition of the boundary layer as deduced from force tests. The results are discussed and compared with theoretical calculations.

The results show that viscosity effects are large and depend to a great degree on the body shape. The effects differ greatly for laminar and turbulent flow in the boundary layer, and within each regime depend upon the Reynolds number of the flow. Laminar flow was found up to a Reynolds number of 6.5 millions and may possibly exist to higher values.

The flow over the afterbody and the shock-wave configuration near the base are shown to be very much different for laminar than for turbulent flow in the boundary layer. The base pressure is much higher with the turbulent layer than with the laminar layer, resulting in a negative base drag in some cases. The total drag characteristics at a given Reynolds number are affected considerably by the transition to turbulent flow. The fore drag of bodies without boat tailing or of boat-tailed bodies for which the effects of flow separation are negligible can be calculated by adding the skin-friction drag based upon the assumption of the low-speed friction characteristics to the theoretical wave drag.

For laminar flow in the boundary layer the effects of varying
the Reynolds number were found to be large, approximately doubling
the base drag in many cases and increasing the total drag about
20 percent over the Reynolds number range investigated. For
turbulent flow in the boundary layer, the effects of varying the
Reynolds number usually changed the base drag and total drag coeffi-
cients considerably.

INTRODUCTION

The effects of viscosity on the aerodynamic characteristics
of bodies moving at low subsonic speeds have been known for many
years and have been evaluated by numerous investigators. The
effects of viscosity at transonic speeds have been investigated
only recently, and relatively large effects on the flow over air-
foils are reported by Ackeret (reference 1) and Liepmann (reference 2).
Although the relative thoroughness of these two investigations has
furnished a good start toward a satisfactory evaluation and under-
standing of the effects of viscosity in transonic flow fields, still
very little is known about the effects at purely supersonic speeds.

The experiments reported in references 3, 4, and 5 have succeeded
in evaluating the magnitude of the skin friction for supersonic flows
in pipes and on curved surfaces. Reference 6 contains a small
amount of data on the effects of Reynolds number on the drag of a
sphere and a circular cylinder; however, these data are not appli-
cable to aerodynamic shapes which are practical for supersonic flight.

It has been generally assumed that the effects of viscosity are
small and need be considered only when determining the magnitude of
skin friction. In reviewing past data for the effects of viscosity
it was found that in many reports, such as references 7 and 8, the
model size was not stated, thereby rendering the calculation of
Reynolds number quite difficult.

Preliminary tests in the Ames 1- by 3-foot supersonic wind
tunnel No. 1, which is a variable-pressure tunnel, showed a relatively
large effect of Reynolds number on the drag of bodies of revolution.
The results of this cursory investigation were not reported because
the magnitude of support interference was not known and because
certain inaccuracies in the balance measurements were known to exist
in the data taken at low tunnel pressures. An investigation of wing-
body interaction at supersonic speeds has been conducted subsequently
and the results presented in reference 9. Because of the support
interference and the balance inaccuracies noted at low pressures
the data presented therein of the effect of Reynolds number on the
drag of smooth bodies are not sufficiently accurate throughout
the range of Reynolds numbers for direct application to the conditions
of free flight.

Since the effects of viscosity already were known to be relatively large at the outset of this investigation, the purpose of the present research was made twofold. The primary purpose was to develop an understanding of the mechanism by which viscosity alters the theoretical inviscid flow over bodies of revolution at supersonic speeds, and the secondary purpose to determine the magnitude of these effects for the particular bodies investigated.

APPARATUS AND TEST METHODS

Wind Tunnel and Instrumentation

A general description of the wind tunnel and the principal instrumentation used can be found in reference 9. Included therein is a description of the schlieren apparatus, which forms an integral part of the wind-tunnel equipment, and the strain-gage balance system employed for measuring aerodynamic forces. In order to obtain accurate data at low as well as high tunnel pressures, a more sensitive drag gage was used in the present investigation than in the investigation of reference 9; however, all other details of the balance system are the same. For the purposes of the present investigation, it is pertinent to add that the tunnel is equipped with three turbulence-reducing screens located in the settling chamber.

The tunnel total pressure, the static reference pressure in the test section, and the pressure in the air chamber of the balance housing were observed on a mercury manometer. Because the difference between the base pressure and the static reference pressure in the test section is ordinarily too small (only 0.5 cm of mercury at low tunnel pressures) to be accurately read from a mercury manometer, a supplementary manometer using a fluid of lower specific gravity was employed. Dibutyl phthalate, having a specific gravity of approximately 1.05 at room temperatures, was used as an indicating fluid in this manometer instead of the conventional light manometer fluids, such as water and alcohol, because of its lower vapor pressure and its property of releasing little or no dissolved air when exposed to very low pressures.

Models and Supports

Photographs of the models, which were made of aluminum alloy, are shown in figures 1 and 2, and their dimensions are given in figure 3. Models 1, 2, and 3 were each formed of a 10-caliber ogive nose followed by a short cylindrical section; they differ from one another only in the amount of boat tailing. The shape of the ogive was not varied in this investigation because the flow over it is not affected appreciably by viscosity. Models 4, 5, and 6, which differ

from one another only in thickness ratio, were formed by parabolic
arcs with the vertex at the position of maximum thickness. For
convenience, some of the more important geometric properties of
models 1 through 6 are listed in the following table:

Model	Frontal area A(sq in)	Nose half angle θ(dog)	Area-volume ratio A/(V)$^{2/3}$	Length-diameter ratio L/D	Base-area ratio A_B/A
1	1.227	18.2	0.302	7.0	1.00
2	1.227	18.2	.309	7.0	.558
3	1.227	18.2	.318	7.0	.348
4	.866	11.3	.305	8.8	.191
5	1.758	15.9	.385	6.2	.186
6	3.426	21.8	.479	4.4	.187

In addition to the above-mentioned models, several other bodies
were tested for certain specific purposes. Thus, models 7 and 8
were made unusually long so that the skin friction would be a large
portion of the measured drag, thereby enabling the condition of the
boundary layer to be deduced from force tests. Various substitute
ogives, shown in figure 2(a), were made interchangeable with the
smooth ogive that is shown attached to the cylindrical afterbody of
model 8. These ogives were provided with different types and
amounts of roughness and could be tested either alone or with the
long cylindrical afterbody attached. When the ogives were tested
alone, a shroud of the same diameter as the ogive was used to
replace the cylindrical afterbody. Model 9, a body with a conical
nose, and model 10, a sphere, were tested in order to compare the
results of the present investigation with existing theoretical
calculations and with the results of other experimental investiga-
tions. Models 11, 12, 13, and 14 were constructed to determine the
effects of the length-diameter ratio for a fixed shape of afterbody.
In all cases when a smooth surface was desired, the models were
polished before testing to obtain a surface as free from scratches
and machining marks as possible.

The models were supported in two different ways: by a rear
support and by a side support, as shown in figures 4, 5, and 6. The
rear support used in the majority of the cases consists of a sting
which supports the model and attaches to the balance beam. A thin
steel shroud encloses the sting and thereby eliminates the aero-
dynamic tare forces. Use of the rear support allows force data, base
pressure data, and schlieren photographs to be taken simultaneously.
The side support which attaches to the lower side of the model
consists of a 6-percent-thick airfoil of straight-side segments
and 7° semiwedge angle at the leading and trailing edges The

side support was used to determine the effects of the axial variation
in test–section static pressure on base pressure, and, in conjunc-
tion with a dummy rear support, to evaluate the effects of support
interference. Base pressure data and schlieren photographs can be
obtained when the side support is used.

Test Methods

The tests were conducted at zero angle of attack in a fixed
nozzle designed to provide a uniform Mach number of approximately
1.5 in the test section. For the positions occupied by the different
models, the free–stream Mach number actually varied from 1.49 to
1.51. This is somewhat lower than the Mach number of the tests
reported in reference 9, which were conducted farther downstream in
the test section.

Before and after each run precautions were taken to test the
pressure lines for leaks and the balance system for friction or
zero shift. Each run was made by starting the tunnel at a low
pressure, usually 3 pounds per square inch absolute, and taking
data at different levels of tunnel stagnation pressure up to a
maximum of 25 pounds per square inch absolute. Because of the lag
in the manometer system, approximately 15 minutes at low pressures
and 5 minutes at high pressures were allowed for conditions to
come to equilibrium. The over–all variation in Reynolds number
based on body length ranged from about 60,000 to 9.4 millions. The
specific humidity of the air usually was maintained below 0.0001
pound of water per pound of dry air, and in all cases was below
0.0003.

In general, each body was tested with a polished surface and
then later with roughness added to fix transition. As illustrated
in figure 2(a), several different methods of fixing transition on
a body in a supersonic stream were tried. The usual carborundum
method employed in subsonic research was not used because of the
danger of blowing carborundum particles into the tunnel–drive
compressors. The method finally adopted was to cement a 1/8–inch–
wide band of particles of table salt around the body. This method
proved successful at all but the very low Reynolds numbers. On
models 1, 2, 3, and 12 roughness was located one–eighth inch down-
stream of the beginning of the cylindrical section. On models 4,
5, and 6 the roughness was placed 4.5 inches from the nose and on
model 8 one–eighth inch upstream of the beginning of the cylindrical
afterbody. Models 7, 9, 10, 11, 13, and 14 were tested in the smooth
condition only.

RESULTS

Reduction of Data

The force data included in this report have been reduced to
the usual coefficient form through division by the product of the
free-stream dynamic pressure and the frontal area of the body.
If it is desired to refer these coefficients to $(volume)^{2/3}$ the
necessary conversion factors can be found in the table of the
geometric properties of the models included in the section on
models and supports. In each case, conditions just ahead of the
nose of a model are taken as the free-stream conditions.

The measurements of the pressure on the base of each model
are referred to free stream static pressure and made dimensionless
through division by the free-stream dynamic pressure. Thus, the
base pressure coefficient is calculated from the equation

$$P_B = \frac{p_B - p_1}{q_1} \tag{1}$$

where

P_B base pressure coefficient

p_B pressure acting on the base

p_1 free-stream static pressure

q_1 free-stream dynamic pressure

The dynamic pressure is calculated from the isentropic relation-
ships. A small experimentally determined correction is applied
for the loss in total pressure due to condensation of water vapor
in the nozzle. The Reynolds number is based upon the body length
and is calculated from the isentropic relationships using
Sutherland's formula for the variation of viscosity with the
temperature of the air.

It is convenient to consider the force due to the base pressure
as a separate component of the total drag. Accordingly, the base
drag is referred to the frontal area, and in coefficient form is
given by

$$C_{D_B} = - P_B \left(\frac{A_B}{A}\right) \tag{2}$$

where

C_{D_B} base drag coefficient

A_B area of base

A frontal area of the body

The fore drag is defined as the sum of all drag forces that act on the body surface forward of the base. Hence, the fore drag coefficient is given by

$$C_{D_F} = C_D - C_{D_B} \qquad (2)$$

where C_D is the total drag coefficient and C_{D_F} the fore drag coefficient. The concept of fore drag coefficient is useful for several reasons. It is the fore drag that is of direct importance to the practical designer when the pressure acting on the base of a body is altered by a jet of gases from a power plant. Considering the fore drag as an independent component of the total drag greatly simplifies the drag analysis of a given body. Finally, the fore drag, as will be explained later, is not affected appreciably by interference of the rear supports used in the investigation.

Since the nozzle calibration with no model present showed that the static pressure along the axis of the test section is not constant (fig. 7), the measured coefficients have been corrected for the increment of drag or pressure resulting from the axial pressure gradient. A detailed discussion of this correction is presented in appendix A, and the experimental justification shown in figures 8 and 9.

Precision

The table which follows lists the total uncertainty that would be introduced into each coefficient in the majority of the results if all of the possible errors that are known to exist in the measurement of the forces and pressures and the determination of free-stream Mach number and gradient corrections were to accumulate. Actually the errors may be expected to be partially compensating, so the probable inaccuracy is about half that given in the table. The sources and estimated magnitudes of the probable errors involved are considered at greater length in appendix B. The values in the following table are for the lowest and highest tunnel pressures and vary linearly in between The table does not apply to data that are presented in figures 12(b), 16, 17 and for models 4, 5, and 6 in

figures 26(a) and 32(a) where the possible variation in the balance
calibration constant may increase the limits of error as discussed
in appendix B.

Coefficient	Maximum value of error at lowest pressure	Maximum value of error at highest pressure
Total drag	± (2.4% plus 0.004)	± (1.1% plus 0.004)
Fore drag	± (1.6% plus 0.004)	± (0.6% plus 0.004)
Base pressure	± (0.8% plus 0.005)	± (0.5% plus 0.005)
Base drag	± [0.8% plus 0.005(A_B/A)]	± [0.5% plus 0.005(A_B/A)]

Effects of Support Interference

Previous to the present investigation an extensive series of
tests was conducted to determine the body shape and support combina-
tions necessary to eliminate or evaluate the support interference.
Based upon the results obtained, a summary of which appears in
appendix C, it is believed that all the drag data presented herein
for the models tested in the smooth condition is free from support
interference effects with the exception of the data shown in figure
30. For the models tested with roughness, the fore drag data are
free from interference effects, but an uncertainty in the base
pressure coefficient exists which may vary from a minimum of ±0.005
to a maximum of ±0.015 for the different bodies. As a result, the
base drag coefficients and total drag coefficients for the same
test conditions are subject to a corresponding small uncertainty.

Schlieren Photographs

Since much of the basic information contained in this report
is obtained from schlieren photographs, a somewhat detailed explana-
tion of their interpretation is in order. A typical schlieren
photograph taken with the knife edge vertical is shown in figure 10.
The various features of the flow are designated in this photograph
which shows the entire field of view of the schlieren apparatus.
Other items, such as the natural gradients inherent in the glass
and the horizontal and vertical reference wires mounted outside of
the tunnel are also apparent in this and other photographs presented
in the report. The horizontal streaks that appear on some of the
schlieren photographs are a result of oil in the tunnel circuit
due to temporarily faulty gasketing in one of the main drive
compressors. The mottled appearance of the background is believed
to result from the varying density gradients in the boundary layer
flow on the glass windows.

The schlieren photographs were taken with the knife edge both
horizontal and vertical. Density gradients normal to the stream

direction are detected with the knife edge horizontal; whereas those
parallel to the stream direction are detected with the knife edge
vertical. For the horizontal orientation the knife edge was placed
so that increasing density gradients in a downward direction appear
as white areas on the photographs. For the vertical orientation
the knife edge was placed (except for the photograph in fig. 10 and
the sphere photographs in fig. 20) so that increasing density
gradients in the downstream direction appear as white areas.

Theoretical Calculations

Although at present no theoretical method is available for
calculating the base pressure and hence the total drag of a body,
several methods are available which provide an excellent theoretical
standard to which the experimental measurements of fore drag can be
compared. In this report the theoretical fore drag is considered
to be the sum of the theoretical wave drag for an inviscid flow and
the skin-friction drag corresponding to the type of boundary layer
that exists on the body.

A typical Mach net and the corresponding pressure distribution
for the theoretical inviscid flow over one of the boat-tailed bodies
tested in this investigation is shown in figure 11. For purposes of
comparison the pressure distribution as calculated by the linear
theory of von Kármán and Moore is included as is the pressure
coefficient at the nose of a cone, the included angle of which is
equal to the angle between the surface tangents at the nose of the
ogive. This latter is obtained by the method of references 10 and 11.

The wave drag for many of the bodies tested was calculated by
the method of characteristics for rotationally symmetric supersonic
flow as given in references 12 and 13. In accordance with the
theoretical results of reference 14, the fluid rotation produced by
the very small curvature of the head shock wave was neglected. This
procedure is justified experimentally in reference 8, where the
theoretical calculation using the method of characteristics as
presented in reference 12 are shown to be in excellent agreement
with the measured pressure distributions for ogives with cylindrical
afterbodies.

The calculation of the skin-friction drag in any given case
requires a knowledge of the condition of the boundary layer. In the
cases for which the schlieren photographs and the force tests indi-
cated that the entire boundary layer was laminar, the curve of
theoretical fore drag used for comparison with the experimental
results was obtained by adding to the wave drag a theoretical
skin-friction drag calculated by using the low-speed skin-friction
coefficients for laminar boundary layer flow at the Reynolds number

based on the full length of the model. This procedure, which is in accordance with reference 3, gives the equation

$$C_{D_f} = C_{f_{lam}}(A_F/A) \qquad (4)$$

where

C_{D_f} skin-friction drag coefficient for the model at the Reynolds number, Re, based on the full length of the model

$C_{f_{lam}}$ low-speed skin-friction coefficient for laminar boundary-layer flow at Re

A_F wetted area of the model forward of the base

A frontal area of the model

For the models with roughness added it was assumed that the disturbance of the boundary layer resulting from the salt band was sufficient to cause transition to a turbulent boundary layer to occur at the band. The theoretical skin-friction drag was then obtained by means of the equation

$$C_{D_f} = C_{f'_{lam}}\left(\frac{A_{lam}}{A}\right) + C_{f_{turb}}\left(\frac{A_F}{A}\right) - C_{f'_{turb}}\left(\frac{A_{lam}}{A}\right) \qquad (5)$$

where

$C_{f'_{lam}}$ low-speed skin-friction coefficient for laminar boundary-layer flow at the effective Reynolds number, Re', based on the length of the model from the nose to the point where the salt band was added

A_{lam} wetted area of that portion of the model forward of the salt band

$C_{f_{turb}}$ low-speed skin-friction coefficient for turbulent boundary-layer flow at the Reynolds number Re, based on the full length of the model

$C_{f'_{turb}}$ low-speed skin-friction coefficient for turbulent boundary-layer flow at the effective Reynolds number Re'

This method of calculation presumes that the fixed roughness was
of such a nature as to cause the turbulent boundary-layer flow
downstream of the point where the roughness was added to be the
same as would have existed had the boundary-layer flow been
turbulent all the way from the nose of the body.

DISCUSSION

Flow Characteristics

Before analyzing the effects of viscosity on the drag of the
bodies of revolution, it is convenient to consider qualitatively
the effects on the general characteristics of the observed flow.
In so doing it is advantageous to consider first the condition of
the boundary layer characterized by whether it is laminar or tur-
bulent and then the effect of variation in Reynolds number on flow
separation for each type of boundary layer. Once the effects, on
flow separation, of the Reynolds number and the condition of the
boundary layer are known, the observed effects on the shock-wave
configuration at the base of the model are easily explained.
Likewise, once the effects on flow separation and shock-wave
configuration are known, the resulting effects of viscosity on
the fore drag, base drag, and total drag are easily understood.

Condition of the boundary layer.- Since results observed at
transonic speeds (references 1 and 2) have shown that the general
flow pattern about a body depends to a marked degree on the type
of boundary layer present, it is possible that the boundary-layer
flow at supersonic speeds also may be of primary importance in
determining the over-all aerodynamic characteristics of a body.
Consequently, the determination of the extent of the laminar
boundary layer under normal test conditions is of fundamental
importance.

In an attempt to determine the highest Reynolds number at which
laminar flow exists on models tested in this investigation, a
relatively long polished body (model 7) was tested from a low
pressure up to the highest tunnel pressure obtainable. In this
case, the diameter of the shroud which encloses the rear support
sting was made the same as the diameter of the body. The fore
drag measurements on this model are shown in figure 12(a). Since
the skin friction is a relatively large portion of the measured
fore drag, the condition of the boundary layer can be deduced from
these force tests. The data indicate that the boundary layer on
this body is still laminar up to the highest obtainable Reynolds
number of 6.5 millions. The computed fore drag data used for
comparison are obtained by adding a laminar or turbulent skin-
friction coefficient based on low-speed characteristics to the

experimental wave drag of the ogival nose. This latter is determined
by subtracting from the fore drag data of figure 16 the low-speed
laminar skin-friction coefficients for the smooth ogive at the
higher Reynolds numbers where the error, resulting from the assump-
tion of the low-speed coefficients, is a small percent of the
deduced wave drag. Schlieren photographs from which the condition
of the boundary layer may be observed are shown in figure 13. They
confirm the previous finding by showing that transition does not
occur on the body, but begins a short distance downstream from
the base of the model, as indicated by arrow 1 in the photograph.

A close examination of the photographs in figure 13 reveals
that the beginning of transition (arrow 1) is located at the same
point on the support shroud as the waves (arrows 2 and 3) which
originate from a disturbance of the boundary layer. It was found
by measurements on the schlieren photographs that the point of
origin of those waves on the shroud and the intersection with the
shroud of the bow wave, which has been reflected by the test-section
side walls, coincide. This suggests that transition on the shroud
is being brought about prematurely by the reflected bow waves. Addi-
tional evidence that this is not natural transition is obtained in
noting from figure 13 that the point where transition begins does
not move with a change in Reynolds number. If the model were longer
than a critical length, which is about 11 inches for the conditions
of the present tests, these reflected waves would strike the model
somewhere on the afterbody and premature transition would be expected
to affect the results. Figure 12(b) shows the results of the
measurements of fore drag on a 16.7-inch body (model 8), which is
considerably longer than the critical length. These force data
confirm the above conjecture by clearly indicating a partially
turbulent boundary layer on the body even at Reynolds numbers as
low as 2 millions. The schlieren photographs of the flow over this
body are presented in figure 14. It is seen that, in this case also,
the transition to turbulent flow (arrow 1) is located at the same
point as the waves (arrows 2 and 3) originating from the disturbance
of the boundary layer by the reflected bow wave. Similarly, an
additional small wave (arrow 4) can be traced back to a disturbance
of the boundary layer caused by a shock wave originating from a
very slightly imperfect fit of the glass windows in the side walls.

Although the maximum possible extent of laminar flow that may
be expected on bodies of revolution cannot be determined on the
basis of the present tests because of this interference from the
reflected shock waves, the foregoing results show that, under the
conditions of those tests, a laminar boundary layer exists over the
entire surface of a smooth model about 11 inches long up to at least
6.5 millions Reynolds number.

In comparison to the values normally encountered at subsonic
speeds, a Reynolds number of 6.5 millions at first appears to be

somewhat high for maintenance of laminar flow over a body, unless favorable pressure gradients exist over the entire length of that body. The pressure distribution over model 7, shown in figure 15, has been determined by superimposing the pressure distribution which exists along the axis of the nozzle with no model present upon the theoretical pressure distribution calculated for model 7 by the method of characteristics. The resulting pressure distribution shows that the pressure gradient is favorable over the ogive, but is actually adverse over the cylindrical afterbody. This suggests that the stability of the laminar boundary layer at a Mach number of 1.5 may be considerably greater than at low Mach numbers.

An increase in the stability of the laminar boundary layer with an increase in Mach number has been indicated previously by the theoretical work of references 15 and 16, and is confirmed experimentally for subsonic flows by the results of references 6 and 17 as well as by the experimental data given for airfoils in reference 15. Some of the experimental research carried out in Germany are in disagreement with these results. In fact, part IV of reference 18 reports that the schlieren observations made in the supersonic wind tunnels at Kochel indicated that the Reynolds number of transition to turbulent flow on cones was even less than the value for an incompressible flow with no pressure gradient. On the basis of the description of the Kochel wind tunnels given in part I of reference 18, it appears that because of several factors the conditions of flow therein are somewhat adverse to the formation of laminar boundary layers as extensive as those that would exist in free flight. One of the more important of these factors is believed to be the large number of shock waves which originate from imperfections in the nozzle walls and disturb the boundary layer over the body. These shock waves ordinarily number about 15 and are readily visible in various schlieren photographs. (See reference 21, for example.)

In order to cause the laminar boundary layer to become turbulent in this investigation, an artifice such as adding roughness was necessary. In a supersonic stream, however, the addition of roughness to a body also will increase the wave drag of that body. The magnitude of the wave drag due to roughness was determined by testing with full diameter shrouding and no afterbody attached, first the smooth ogive, and then the ogives with various amounts and kinds of roughness added (fig. 2(a)).

The corresponding fore drag measurements are shown in figure 16. These data illustrate that little additional drag is attributable to roughness at the low Reynolds numbers where the boundary layer is relatively thick, but that an appreciable amount of wave drag is attributable to it at the higher Reynolds numbers. For all subsequent results presented, the amount of drag caused by the artifical roughness is subtracted from the measured data taken for the bodies

tested with transition fixed. In order to calculate the amount of
drag caused by the roughness for models of diameters different from
the ogives tested, it was assumed that for any model the increment
in drag coefficient attributable to the drag of the artificial
roughness was inversely proportional to the diameter of the model,
at the station at which the roughness was applied.

The fore drag measurements of model 8, which consists of a
cylindrical afterbody with any one of the interchangeable ogives
directly attached, are presented in figure 17. These data, from
which the drag increment due to the added roughness has been sub-
tracted as noted previously, show that the degree of roughness
produced by sand blasting the surface of the ogive is insufficient
to cause transition at low Reynolds numbers; whereas, the roughness
produced by the 3/16-inch- or the 3/8-inch-wide salt band caused
transition at all Reynolds numbers.

A vivid illustration of the turbulent character of the boundary
layer on those bodies with roughness added is given by the schlieren
photographs in figure 18. The boundary layer is best seen in the
photograph taken with the knife edge horizontal. A comparison of
these photographs with those of laminar boundary layers (fig. 13,
for example) illustrates how the condition of the boundary layer is
apparent from schlieren photographs.

The results at transonic speeds reported in references 1 and 2
have shown that the same changes in pressure distribution and shock-
wave configuration brought about by transition due to inherent
boundary-layer instability at high Reynolds numbers can also be
brought about at those speeds by any of several means. The artifices
used in references 1 and 2 included fine-grain roughness, free-
stream turbulence, and a single large disturbance; the resulting
aerodynamic effects were the same, provided in each case the boundary
layer was changed from laminar to turbulent. Consequently, no
matter what causes the boundary layer to become turbulent in free
flight, it seems likely that, excluding possible small differences
in skin friction, the resulting effects on the aerodynamic character-
istics of the body will be very nearly the same as if the boundary
layer were made turbulent by roughness alone, as is the case in the
experiments conducted in this investigation.

Flow Separation.- Changes in flow separation brought about by
changing the boundary-layer flow from laminar to turbulent alter
the effective shape of the body, the shock-wave configuration, and
also the drag. It is therefore essential to consider the effects
on flow separation of both the condition of the boundary layer and
the Reynolds number.

The location and degree of separation of the laminar boundary
layer for the boat-tailed bodies tested in the smooth condition

varied noticeably with the Reynolds number of flow. The schlieren photographs of Model 6 in figure 19 are typical of this effect. Additional photographs, presented in figure 20, illustrate the same phenomena in the flow over models 2, 3, and 10, each at two different Reynolds numbers. In each case, as the Reynolds number of the flow is increased, the separation decreases, the convergence of the wake increases, and the trailing shock wave moves forward.

Separation of an apparently laminar boundary layer has been pointed out previously by Ferri in reference 19 for the two-dimensional supersonic flow over the surface of curved airfoils. The schlieren photographs therein indicate that a shock wave forms at the point of laminar separation. On the other hand, the schlieren pictures of the flow fields for the bodies of revolution tested in the present investigation, show no definite shock wave accompanying separation except for the sphere (fig. 20) in which case the shock wave is very weak indeed. It may be concluded, therefore, that a separation of the laminar boundary layer is not necessarily accompanied by a shock wave at supersonic speeds. The same con clusion for transonic flows has been drawn in reference 2.

It might be surmised that the trailing shock wave situated some distance downstream of the separation point is interacting with or, perhaps, even causing the flow separation by virtue of pressure disturbances propagated upstream through the subsonic portion of the wake and boundary layer. Some indication that this is not the case is given by the schlieren photographs in figures 19 and 20. It can be seen from these photographs that the trailing shock wave moves upstream and the point of separation moves downstream as the Reynolds number is increased. It would logically be expected that this decrease in the distance between the shock wave and the separation point would intensify any possible interaction between these two elements. The photographs show, however, that the degree of separa tion actually decreases as the trailing shock wave moves upstream. This suggests that the trailing shock wave does not have much influence on the laminar separation. Additional evidence which corroborates this conjecture was noted in the course of the investigation of support interference, wherein it was found that if the diameter of the support behind models 2 and 3 was increased, the trailing shock wave moved forward, but the base pressure and laminar separation did not change. On this basis it appears likely that the cause of the laminar separation is not associated with a shock wave, but with other phenomena.

In order to analyze more closely the details of the flow separation, the pressure distribution along the streamline just outside of the separated boundary layer was calculated for several flow conditions over models 3 and 6. The calculations were made using the method of characteristics, and obtaining the contour of the streamline just outside the separated boundary layer from enlargements of the schlieren photographs. Typical results from

these calculations for model 3 are presented in figure 21. It is
seen that the pressure on the outside of the boundary layer is
approximately constant, downstream of the point of separation, as
is characteristic along the boundary of a "dead-water" region. The
pressure along the line of separation can be expected to be approxi-
mately equal to that in the dead-water region, and hence, equal to
the base pressure. A comparison of the calculated values of the
average pressure in the dead-water region with the measured values
of the base pressure for several conditions of flow over models 3
and 6 is given in the following table:

Model	Reynolds number	Calculated pressure coeffi- cient of dead water region	Measured base pressure coefficient
3	0.6×10^6	−0.06	−0.06
3	2.0×10^6	−.11	−.12
6	$.6 \times 10^6$	−.10	−.11
6	1.5×10^6	−.13	−.13

The preceding results indicate that for laminar flow the base pressure,
at least for boat-tailed bodies, is determined by the degree of
separation which occurs forward of the base. This suggests that,
if a means can be found to control the separation, the base pressure
also can be controlled.

The theoretical pressure distributions on models 4 and 5 are
similar to the pressure distribution on model 6, which is shown in
figure 22. In each case, the laminar separation observed in the
schlieren photographs is located at a point upstream of which the
pressure decreases continually along the direction of flow. For
subsonic flow this condition ordinarily would be termed favorable
and separation would not be expected. It thus appears that the
separation phenomena observed are of a different nature from those
which commonly result from a retardation of the fluid particles in
the boundary layer. Further research on this subject is necessary
in order to gain a satisfactory understanding of the observed results.

The findings of previous investigations in low-speed flows
indicate that if a boundary layer which is normally laminar over
the afterbody is made turbulent by either natural or artificial
means, the resistance to separation is increased greatly. The tests
on models 2, 3, 4, 5, and 6 with roughness added show clearly that
this is also the case in supersonic flows. The two schlieren
photographs presented in figure 23 were taken of model 6 with and
without roughness added and are typical of this effect. A compari-
son of the two photographs shows that, without roughness added,
separation occurs near the point of maximum thickness, but if
transition is fixed ahead of this point such separation no longer
occurs.

Shock-wave configuration. - It is to be expected that the changes
in flow separation due to changes in the condition of the boundary
layer and in the Reynolds number of the flow will bring about changes
in the shock-wave configuration at the base of a body. The schlieren
photographs of figures 19 and 20, which show how the laminar separa-
tion decreases and the convergence of the wake increases as the
Reynolds number is increased, also show that those phenomena are
accompanied by a forward motion of the trailing shock wave. In
general, as long as the boundary layer is laminar, the trailing
shock wave moves forward as the Reynolds number increases, but no
major change in the shock-wave configuration takes place.

The shock-wave configuration with a turbulent boundary layer,
however, is very much different from the configuration with a
laminar layer, as is illustrated by the schlieren photographs of
model 6, shown in figure 23. Such configuration changes due to
the transition to turbulent boundary-layer flow correlate quite
well with the angle β that the tangent to the surface just ahead
of the base makes with the axis of symmetry. Figure 24 shows the
changes in shock-wave configuration for models 1 through 6 arranged
in order of increasing angle β. It is seen that, on the boat-
tailed bodies with a small angle β, the transition to a turbulent
boundary layer is accompanied by the appearance of a weak shock
wave originating at the base of the body (models 4 and 2). For
bodies with larger boat-tail angles (model 5) the strength of this
wave, hereafter termed the "base shock wave," increases until it is
approximately as strong as the original trailing shock wave. For
even larger boat-tail angles, the base shock wave becomes more
distinct, and eventually is the only appreciable shock wave exist-
ing near the base of the body (models 3 and 6). In such a case,
the compression through the base shock wave occurs forward of the
base. This, as will be shown later, greatly increases the base
pressure and decreases the base drag. Since the change in shock-
wave configuration caused by the addition of roughness is due to
the greater resistance to flow separation of the turbulent boundary
layer, it may be expected that the above shock-wave configurations
for the turbulent boundary layer will be obtained regardless of the
cause of transition.

Compared to the phenomena observed with a laminar boundary layer
(fig. 19), changes in the Reynolds number for a body with a turbulent
boundary layer do not alter the shock wave configuration to any
significant extent, because the turbulent layer, even at low
Reynolds numbers, ordinarily does not separate. This fact is evident
in figure 25, which shows the schlieren photographs of model 3 at
different Reynolds numbers with roughness added. No apparent change
in the flow characteristics takes place as the Reynolds number is
increased. With a turbulent boundary layer, therefore, the effect
on base drag of varying the Reynolds number may be expected to be
much less than with a laminar layer.

Analysis of the Drag Data

The qualitative effects of viscosity on flow separation and on shock-wave configuration, which have been discussed in the preceding sections, provide the physical basis for understanding the effects of varying the Reynolds number and changing the condition of the boundary layer on the drag coefficients of the various bodies tested.

Fore drag.— The fore drag coefficients of models 1 through 6 with laminar flow in the boundary layer are shown in figure 26(a) as a function of the Reynolds number. These data show that, over the Reynolds number range covered in the tests, the fore drag of model 1 decreases about 20 percent, while that of model 6 increases about 15 percent. The fore drag of the other bodies does not change appreciably.

The reason the effects of Reynolds number vary considerably with different body shapes is clearly illustrated by a comparison of the measured fore drags with the theoretical fore drags. In figure 27(a) the theoretical and measured values of fore drag are compared for model 1, which has no boat tailing, and for model 3, which is typical of the boat-tailed models. From this comparison, it is seen that, as previously noted for other models without boat tailing, the theoretical and experimental fore drags for model 1 are in good agreement. The decrease in fore drag with increasing Reynolds number for the bodies without boat tailing is due entirely to the decrease in skin-friction coefficient. For model 3, which has considerable boat tailing, the curves of figure 27(a) show that the theoretical and experimental fore drags agree only at high Reynolds numbers. At the low Reynolds numbers the measured fore drags are lower than the theoretical values because of the separation of the laminar boundary layer as previously illustrated by the schlieren photographs in figures 19 and 20. With separation, the flow over the boat tail does not follow the contour of the body, and the pressure in the accompanying dead-water region is higher than it would be if the separation did not occur (fig. 21). This makes the actual fore drag lower than the theoretical value for a flow without separation. At the higher Reynolds numbers, the separation is negligible and the flow closely follows the contour of the body; hence, the theoretical and experimental fore drags agree. The reason for the approximately constant fore drag of models 2, 3, 4, and 5, therefore, is that the changes due to skin friction and flow separation are compensating. For model 6 with a smooth surface, the fore drag shown in figure 26(a) rises rather rapidly at low Reynolds numbers because the separation effects for this relatively thick body (fig. 19) more than compensate for the changes in skin friction due to the variation of the Reynolds number.

Figure 26(b), which shows the fore drag coefficients of models 1 through 6 with roughness added, indicates that the fore drag for all the bodies decreases as the Reynolds number increases above a

Reynolds number of 1.75 millions. This is to be expected, since with the change to turbulent boundary layer and consequent elimination of separation, the only factor remaining to influence the fore drag coefficients is the decrease of skin-friction coefficients with increase in Reynolds number. Below a Reynolds number of 1.75 millions, however, the fore drag of all the models except model 1 increases with increasing Reynolds number. The cause of this somewhat puzzling behavior is apparent upon closer examination of the data.

Figure 27(b) shows a comparison of the theoretical fore drags with the experimental values for models 1 and 3 with roughness added. The theoretical value for skin-friction drag was calculated assuming laminar flow up to the location of the roughness, and turbulent flow behind it. This value of drag was added to the theoretical wave drag to obtain the theoretical fore drag. It is seen from figure 27(b) that for model 1 the curves of theoretical and experimental fore drag have the previously indicated trend of decreasing drag with increasing Reynolds number over the entire range. However, for model 3, which is typical of the boat-tailed bodies, the measured fore drag at low Reynolds numbers falls considerably below the theoretical value in the manner previously noted. The reason for this is evident from an examination of the schlieren photographs shown in figure 28, which were taken of the flow over models 3 and 6 with roughness added. They show that at the low Reynolds numbers a flow separation similar to that observed for an undisturbed laminar boundary layer (fig. 19) is evident, and the resulting shock-wave configuration is characteristic of the configuration for a laminar boundary layer rather than that for a turbulent boundary layer. It appears that, at the low Reynolds numbers, the amount of roughness added does not cause transition far enough upstream of the point for laminar separation so that the free stream can provide the boundary layer with the necessary additional momentum to prevent separation. The portions of the drag curves in which the desired transition was not realized are shown dotted over the region in which separation was apparent from the schlieren pictures. For model 1, the schlieren photographs showed that at the low Reynolds numbers the amount of roughness added was sufficient to effect transition some distance ahead of the base, although not immediately aft of the roughness.

The agreement between the experimental and the theoretical results obtained by the use of equations (4) and (5) indicates that, at a Mach number of 1.5 and in the range of Reynolds numbers covered by this investigation, the familiar low-speed skin-friction coefficients can be used to estimate drag due to skin friction at supersonic speeds. This confirms the results of references 3, 4, and 5 and extends their application to the evaluation of skin-friction drag for supersonic flow on bodies of revolution.

A comparison of the curves of figures 26(a) and 26(b) shows
that for a given body at a given value of the Reynolds number the
fore drag with roughness added is consistently higher than the
corresponding fore drag of the smooth-surfaced body. In the
general case, this over-all increase in fore drag is attributable
both to the increase in the skin-friction drag of the body and to
the elimination of separation with consequent increase in the
pressure drag of the boat tail. For model 1, which has no boat
tailing, the increase in skin friction is the sole factor contribut-
ing to the increase in fore drag.

Base pressure and base drag.-- Figure 29(a) shows the base
pressure coefficients plotted as a function of the Reynolds number
for models 1 through 6, each with a smooth surface. It is evident
from the data in this figure that the effects of Reynolds number on
base pressure for a body with a laminar boundary layer are quite large.
In the range of Reynolds numbers covered, the base pressure coeffi-
cient of model 1 increases about 60 percent, and the coefficients of
models 2, 3, and 4 more than double. The thicker bodies, models 5
and 6, do not exhibit such large changes in base pressure coefficient,
for the coefficients apparently reach a maximum at a relatively low
Reynolds number, and then decrease with further increase in the
Reynolds number.

The base pressure coefficients for models 1 through 6 with
roughness added are shown in figure 29(b). Here again, the portions
of the curves which correspond to the low Reynolds number region
wherein transition did not occur far enough upstream to prevent
separation are shown as dotted lines. Model 1 exhibits the lowest
base pressure and model 6 the highest; in this latter case the base
pressure is even higher than the free-stream static pressure. The
physical reason for this is evident from the schlieren photograph
at the bottom of figure 23, which shows that a compression through
the shock wave occurs just ahead of the base of model 6. Except
for the large changes in pressure coefficient at low Reynolds
numbers where the desired transition was not effected, the variation
of base pressure coefficient with Reynolds number is relatively
small for the bodies with roughness added.

From a comparison of the curves for the bodies with roughness
added to the corresponding curves for the smooth-surfaced bodies,
it is evident that a large change in the base pressure coefficient
is attributable to the change in the condition of the boundary
layer. In general, the base pressures for bodies with roughness
added are considerably higher than the corresponding base pressures
for the smooth-surfaced bodies. In the case of the boat-tailed
bodies the physical reason for this increase in the base pressure
is the appearance of the base shock wave, as shown in figure 24.
For model 1, which has no boat tailing, the mixing action and
greater thickness of the turbulent boundary layer are probably

responsible for the observed increase.

The foregoing data show that the effects of Reynolds number and condition of the boundary layer on the base pressure of a body moving at supersonic speeds depend considerably upon the shape of the after-body. In order to ascertain whether the effects of viscosity also depend upon the length-diameter ratio for a fixed shape of afterbody, some models of different length diameter ratios were tested and the data presented in figures 30(a) and 30(b) which show the variation of base pressure coefficient with Reynolds number. The data presented in this figure are not free of support interference. From these data it is apparent that the effects of viscosity on the base pressure increase with the length-diameter ratio of the body. It is to be noted that the base pressure increases as the length diameter ratio increases. This is somewhat at variance with the results of reference 20 (also reported in reference 18), which showed an effect, but not a systematic one, of length-diameter ratio on the base pressure of bodies without boat tailing.

The base drag coefficient can be obtained from the base pressure coefficient of the models by using equation (2). The base drag coefficients for the smooth-surfaced bodies are presented in figure 31(a) and for the bodies with roughness added in figure 31(b). These curves are, of course, similar to the corresponding curves of base pressure coefficient given in figures 29(a) and 29(b). In this form the ordinates can be added directly to the fore drag coefficients of figure 26 to obtain the total drag coefficient of a given body. It is seen that the contribution of the base pressure to the total drag is very small for models with large amounts of boat tailing, such as models 3, 4, 5, and 6.

Total drag.- The total drag coefficients for models 1 through 6 with smooth surfaces are shown in figure 32(a) as a function of Reynolds number. These data show that the drag coefficients of both models 1 and 2 with a laminar boundary layer increase a little over 20 percent from the lowest to the highest value of Reynolds number obtained in the tests. The other models exhibit somewhat smaller changes. The data presented in figures 26 and 31 indicate that the principal effect controlling the variation of total drag with Reynolds number for laminar flow in the boundary layer is the effect of Reynolds number on the base drag of the bodies. For the special case of highly boat-tailed bodies, however, this effect is of little relative importance because the base drag is a small part of the total drag. In such cases, the over-all variation of drag coefficient is due almost entirely to the variation of fore drag with Reynolds number.

Figure 32(b) shows the total drag coefficients plotted as a function of the Reynolds number for models 1 through 6 with rough-ness added. Again, the portions of the curves that are shown dotted

represent the Reynolds number region in which the amount of roughness
added is insufficient to cause transition far enough upstream so that
separation is prevented. All the curves have approximately the same
trend, the over-all effect on the drag coefficients being about 15
percent or less for the various bodies.

A comparison of the curves of total drag for bodies with rough-
ness added to the corresponding curves for bodies with smooth surfaces
shows an interesting phenomenon. At the higher Reynolds numbers the
drag of models 1 and 6 is actually decreased slightly by the addition
of roughness, in spite of the corresponding increase in skin-friction
drag. The reason is, of course, that the base drags are very much
lower for the turbulent boundary layer than for the laminar. The
drag coefficients of the other bodies (models 2, 3, 4, and 5) are
somewhat higher with roughness added, because the increase in friction
drag of the turbulent boundary layer is greater than the decrease in
base drag.

The importance of always considering both the Reynolds number of
the flow and condition of the boundary layer is illustrated by the
total drag characteristics of model 2. For example, if model 2 were
tested with a turbulent boundary layer at a Reynolds number of 2
millions, the drag would be about 35 percent higher than if tested
with a laminar boundary layer at a Reynolds number of one-half
million. Although discrepancies as large as these have not been
reported as yet in the drag data from different supersonic wind
tunnels, certain consistent differences, varying from about 5 to 25
percent, have been reported (reference 21) in the drag data of
similar projectiles tested in the Gottingen and the Kochel tunnels.
Although in reference 21 the discrepancies between the two tunnels
were attributed only to the variation in skin friction with Reynolds
number, it appears from the results of the present investigation
that such discrepancies are attributable primarily to differences
in flow separation and base pressure.

A comparison of the effects of viscosity for pointed bodies
with the effects for a blunt body shows clearly that body shape
must be considered, and that conclusions about viscosity effects
based upon tests of blunt bodies may be completely inapplicable
to the aerodynamic shapes which are suitable for supersonic flight.
For example, in the case of a sphere at 1.5 Mach number with an over-
all Reynolds number variation of from 7.5×10^4 to 9.0×10^5, the
agreement between the drag data from Gottingen (reference 7),
Peenemunde (reference 21), and the present wind tunnel is within 1
percent of the values measured for free-flight (references 7 and 22).
It is evident that the effects of viscosity on the drag of a sphere
are quite different from the effects on the pointed bodies tested
in this investigation.

CONCLUSIONS

The conclusions which follow apply for a Mach number of 1.5 and at Reynolds numbers based upon model length up to about 5 millions for bodies of revolution similar to the ones tested.

1. The effects of viscosity differ greatly for laminar and turbulent flow in the boundary layer, and within each regime depend upon the Reynolds number of the flow and the shape of the body.

2. Laminar flow was found on the smooth bodies up to a Reynolds number of 6.5 millions and may possibly exist to considerably higher values.

3. A comparison between the test results for laminar and for turbulent flow in the boundary layer at a fixed value of the Reynolds number shows that:

(a) The resistance to separation with turbulent flow in the boundary layer is much greater.

(b) The shock-wave configuration near the base depends upon the type of the boundary-layer flow and the relative degree of boat tailing.

(c) The fore drag coefficients with turbulent boundary layer ordinarily are higher.

(d) The base pressure is much higher with the turbulent boundary layer.

(e) The total drag is usually higher with the turbulent boundary layer.

4. For laminar flow in the boundary layer the following effects were found:

(a) The laminar boundary layer separates forward of the base on all boat-tailed bodies tested, and the position of separation varies noticeably with Reynolds number. Laminar separation is not necessarily accompanied by a shock wave originating from the point of separation. On many of the models the separation is located in a region upstream of which the pressure continually decreases in the direction of the flow.

(b) The trailing shock wave moves forward slightly as the Reynolds number is increased, but no significant change takes place in the shock-wave configuration near the base.

(c) With increasing Reynolds numbers, the fore drag coeffi-
cients increase for highly boat-tailed bodies and
decrease for bodies without boat tailing. For moder-
ately boat-tailed bodies the variation of the fore
drag coefficient with Reynolds number is relatively
small.

(d) The base pressure of the boat-tailed bodies is
controlled by the laminar separation and changes
markedly with Reynolds number. For bodies with
the same afterbody shape, the base pressure also
depends upon the length-diameter ratio of the body.

(e) Total drag varies considerably with Reynolds number,
changing more than 20 percent for several of the
models.

5. For turbulent flow in the boundary layer the following effects
were found:

(a) Separation does not ordinarily occur.

(b) The shock-wave configuration near the base does not
change noticeably as the Reynolds number changes.

(c) The fore drag coefficients decrease slightly as the
Reynolds number is increased.

(d) The base pressure changes very little with changing
Reynolds number.

(e) The total drag decreases as the Reynolds number is
increased.

Ames Aeronautical Laboratory,
   National Advisory Committee for Aeronautics,
      Moffett Field, Calif.

APPENDIX A

VARIATION OF TEST-SECTION STATIC PRESSURE

Since the static pressure with no model present varied along the axis of the test section as shown in figure 7, it was necessary to apply a correction to the measured coefficients to account for the increment in drag or pressure resulting from this axial pressure gradient. Although the axial variation of test-section static pressure is not monotonic, the pressures at the downstream end of the test section are uniformly lower than the pressures of the upstream end where the nose of the models are ordinarily placed. This means that the actual pressure exerted at a given point on a body is lower than it would be if the ambient pressure gradient were zero as it is in free flight. The gradient corrections are calculated on the assumption that the magnitude of the pressure exerted at an arbitrary point on the body in the tunnel is lower than it would be if no gradient were present by an increment equal to the amount which the static pressure decreases (with no model present) from the position of the model nose to the position of the arbitrary point. It is not necessary to include the corresponding axial variation of dynamic pressure in the corrections since it varies only ±0.2 percent from the mean test-section value used in all calculations. The corrections to the measured coefficients of model 1 located 2.5 inches downstream from the reference pressure orifice, for example, amount to +0.012 in fore drag coefficient and −0.026 in base drag coefficient; the corresponding percentages of the uncorrected coefficients of fore drag and base pressure are 12 and 15, respectively.

Because the gradient correction is relatively large in the present tests and apparently has not been applied in the past to supersonic wind-tunnel data, an experimental justification of such theoretical corrections is in order. The validity of the corrections as applied to fore drag is confirmed by tests on model 9, which consists of a conical nose with a 20° included angle and a short cylindrical afterbody. The theoretical fore drag of this body, which is equal to the sum of the wave and friction drags, can be easily calculated as a function of Reynolds number. The wave drag of the conical nose is given accurately by the experimentally confirmed calculations of Taylor and Maccoll (references 10 and 11). The frictional drag can be calculated using the low-speed laminar skin-friction coefficients in accordance with references 3 and 11, since the boundary layer was completely laminar over this model. A comparison of the corrected and uncorrected fore drags with the theoretical fore drag is shown in figure 8. The corrected fore drag coefficients are seen to be in good agreement with the theoretical values; whereas the uncorrected data fall below the wave drag at high tunnel pressures. This latter condition, of course, represents an impossible situation for a body without boat tailing.

In order to check experimentally the validity of the corrections
as applied to the measured base pressure, model 1 was tested on the
side support at five different positions along the axis of the test
section. Because the support system remained fixed relative to the
body, the interference of the support is the same in each case, hence,
any discrepancies in the measured base pressures at the various
positions are attibutable only to the pressure gradient along the
tunnel axis. Figure 9 shows that the uncorrected base pressure data
taken at the five different positions differ by about 25 percent, but
the corresponding five sets of corrected data fall within about ±1.5
percent of their mean, thus confirming the validity of the correction.

APPENDIX B

PRECISION OF DATA

The accuracy of the results presented can be estimated by considering the possible errors that are known to be involved in the measurement of the forces and pressures, and in the determination of the free-stream Mach number and gradient corrections.

The force measurements are subject to errors from shifts in the balance zero due to temperature effects, and also from a shift in the calibration constant. The zero shift, which is less than ± 1 percent of the force data at low pressures and less than ± 0.2 percent at high pressures, was checked periodically by running the tunnel through the complete temperature range with no force applied to the balance. In the majority of cases the variation of the balance calibration constant, which was checked before and after each series of tests, permitted a possible deviation of ± 0.3 percent in the force data. All data presented in figures 12(b), 16, 17, and the data for models 4, 5, and 6 in figures 26(a) and 32(a) were obtained during a period between two consecutive balance calibrations for which the constant differed by 6.4 percent. A comparison of the data obtained during this period with theoretical results and with the results of subsequent reruns of some of the same models indicates that the change in balance calibration occured before the data in question were obtained. The results in the aforementioned figures were therefore computed on the basis of the later calibration. It is estimated that the maximum error in the balance calibration constant for these results is at worst no greater than +0.3 to −3.0 percent.

The pressure data, including the dynamic pressure, are subject to small errors resulting from possible inexact readings of the mercury manometers. The base pressure data are also subject to an additional error resulting from the small variation in the specific gravity of the dibutyl phthalate indicating fluid. At the most, these sources can cause an error in the total and fore drag coefficients of about ± 0.3 percent, and in the base drag coefficient of about ± 0.8 percent. The error in dynamic pressure due to the uncertainty in the free-stream Mach number is negligible, since the isentropic relation for the dynamic pressure as a function of Mach number is near a maximum at a Mach number of 1.5. For slender bodies of revolution the variation of the force coefficients with Mach number is quite small; hence, errors resulting from the variation of free-stream Mach number from 1.49 to 1.51 are negligible.

On the basis of the data presented in figures 8 and 9, it is estimated that for all tunnel pressures the uncertainty in the gradient corrections to total drag, fore drag, and base pressure coefficients can cause at the most an error in these coefficients

of ±0.004, ±0.004, and ±0.005, respectively. It should be noted that in the table on precision, presented in the section on results, this source of error, which is independent of tunnel pressure, is expressed as an increment and not as a percentage of the measured coefficient.

Previous investigations have shown that an uncertainty may be introduced in supersonic wind-tunnel data if the humidity of the tunnel air is very high. To determine the effects of this variable in the present investigation, the specific humidity was varied from the lowest values (approximately 0.0001) to values approximately 20 times those normally encountered in the tests. Drag and base pressure measurements were taken on a body with a conical head and also on a sphere. The results showed no appreciable effect of humidity over a range much greater than that encountered in the present tests, provided the variation in test-section dynamic pressure with the change in humidity was taken into account in the reduction of the data. It is believed, therefore, that the precision of the results presented in this report is unaffected by humidity.

APPENDIX C

EFFECT OF SUPPORT INTERFERENCE

A knowledge of the effects of support interference upon the data in question is essential to an understanding of its applicability to free flight conditions. Previous to the present investigation an extensive series of tests were conducted to determine the body shape and support combinations necessary to evaluate the support interference.

In general, it was found that for the models tested in the smooth condition (laminar boundary layer) the effect of the rear supports used in the present investigation was negligible in all respects for the boat-tailed models 2 and 3 and was appreciable only in the base pressure measurements for model 1. On the basis of these results it is believed that the rear supports used for the other highly boat-tailed bodies (models 4, 5, and 6) have a negligible effect on the drag of the model. For model 1 combinations of rear support and side support were used to evaluate the effect of the rear support on the base pressure. The evaluation was made on the assumption of no mutual interference between the rear support and side support, and was checked by the use of two different combinations of side support and rear support. The data indicate that the assumption is justified within the limits of the experimental accuracy and that the corrected, interference-free base pressures deduced by this method differ only slightly from those measured with the side support alone.

For the bodies with roughness added (producing a turbulent boundary layer) a complete investigation of the support interference was not made; consequently, a definite quantitative evaluation of the interference effects for each body in this condition cannot be given. From the data that were obtained it has been found that the fore drag is unaffected by the presence of the supports used in the present investigation, but that a small amount of interference is evident in the base pressure coefficient which may vary from a minimum of ±0.005 to a maximum of ±0.015 for the different bodies. This uncertainty in the base pressure coefficient results in a correspondingly small uncertainty in the base drag coefficient and in the total drag coefficient.

REFERENCES

1. Ackeret, J., Feldmann, F., and Rott, N.: Investigations of
    Compression Shocks and Boundary Layers in Gases Moving at High
    Speed. NACA TM No. 1113, 1947.

2. Liepmann, H.W.: Further Investigations of the Interaction of
    Boundary Layer and Shock Waves in Transonic Flow. Jour. Aero.
    Sci., vol. 13, no. 12, Dec. 1946.

3. Theodorsen, Theodore, and Regier, Arthur: Experiments on Drag
    of Revolving Disks, Cylinders and Streamline Rods at High Speeds.
    NACA ACR No. L4F16, 1944.

4. Keenan, Joseph H., and Neumann, Ernest P.: Friction in Pipes at
    Supersonic and Subsonic Velocities. NACA TN No. 963, 1945.

5. Frosell, W.: Flow in Smooth Straight Pipes at Velocities Above
    and Below Sound Velocity. NACA TM No. 844, 1938.

6. Ferri, Antonio: Influenza del Numero di Reynolds ai Grandi
    Numeri di Mach. Atti di Guidonia No. 67-69, 1942.

7. Walchner, O.: Systematische Geschossmessungen im Windkanal.
    Lilienthal-Gesellschaft für Luftfahrtforschung, Berich 138,
    Teil 1, Oct. 1941

8. Bach, F.: Druckverteilungsmessungen an Geschossmodellen.
    Deutsche Luftfahrtforschung, UM 6057, Mar. 1945

9. Van Dyke, Milton D.: Aerodynamic Characteristics Including
    Scale Effect of Several Wings and Bodies Alone and in Combina-
    tion at a Mach Number of 1.53. NACA RM No. A6K22, 1946.

10. Maccoll, J.W.: The Conical Shock Wave Formed by a Cone Moving
    at a High Speed. Proc. of the Royal Soc. of London, ser. A,
    vol. 159, Apr. 1, 1937.

11. Taylor, G.I., and Maccoll, J.W.: The Air Pressure on a Cone
    Moving at High Speeds, Proc. of the Royal Soc. of London,
    ser. A, vol. 139, Feb. 1, 1933.

12. Sauer, R.: Method of Characteristics for Three-Dimensional
    Axially Symmetrical Supersonic Flows. NACA TM No. 1133, 1947.

13. Sauer, R.: Theoretische Einführung in die Gasdynamik. Berlin,
    Springer, 1943 (Reprinted by Edwards Bros., Ann Arbor, Mich.,
    1945.)

14. Tollmein, W., and Schäfer, M.: Rotationssymmetrische
    Überschallströmungen. Lilienthal-Gesellschaft für
    Luftfahrtforschung, Bericht 139, Teil 2, Oct., 1941.

15. Allen, H. Julian, and Nitzberg, Gerald E.: The Effect of
    Compressibility on the Growth of the Laminar Boundary Layer
    on Low-Drag Wings and Bodies. NACA ACR, Jan. 1943.

16. Lees, Lester, and Lin, Chia Chiao: Investigation of the
    Stability of the Laminar Boundary Layer in a Compressible
    Fluid. NACA TN No. 1115, 1946.

17. Matt, H.: Hochgeschwindigkeitsmessungen an Rund-und
    Profilstangen verscheidener Durchmesser. Lilienthal-
    Gesellschaft für Luftfahrtforschungen, Bericht 156, Oct. 1942.

18. Owen, P.R.: Note on the Apparatus and Work of the W.V.A.
    Supersonic Institute at Kochel, S. Germany. Part I, (RAE TN NO. 1711)
    Oct. 1945, and Part IV, (RAE TN NO. 1742) Jan. 1946. (British/U.S.
    Restricted).

19. Ferri, Antonio: Experimental Results with Airfoils Tested in
    the High-Speed Tunnel at Guidonia. NACA TM No. 946, 1940.

20. Erdmann, S.: Widerstandsbestimmung Von Kegeln und Kugeln
    aus der Druckverteilung bei Überschallgeschwindigkeit.
    Lilienthal-Gesellschaft für Luftfahrtforschungen, Bericht 139,
    Teil 2, Oct. 1941.

21. Lehnert, R.: Systematische Messungen an neun einfachen
    Geschossformen im Vergleich zu Messungen der AVA-Göttingen.
    Lilienthal-Gesellschaft für Luftfahrtforschungen, Bericht 139,
    Teil 2, 1941.

22. Charters, A.C., and Thomas, R.N.: The Aerodynamic Performance
    of Small Spheres from Subsonic to High Supersonic Velocities.
    Jour. Aero. Sci., vol. 12, no. 4, Oct. 1945.
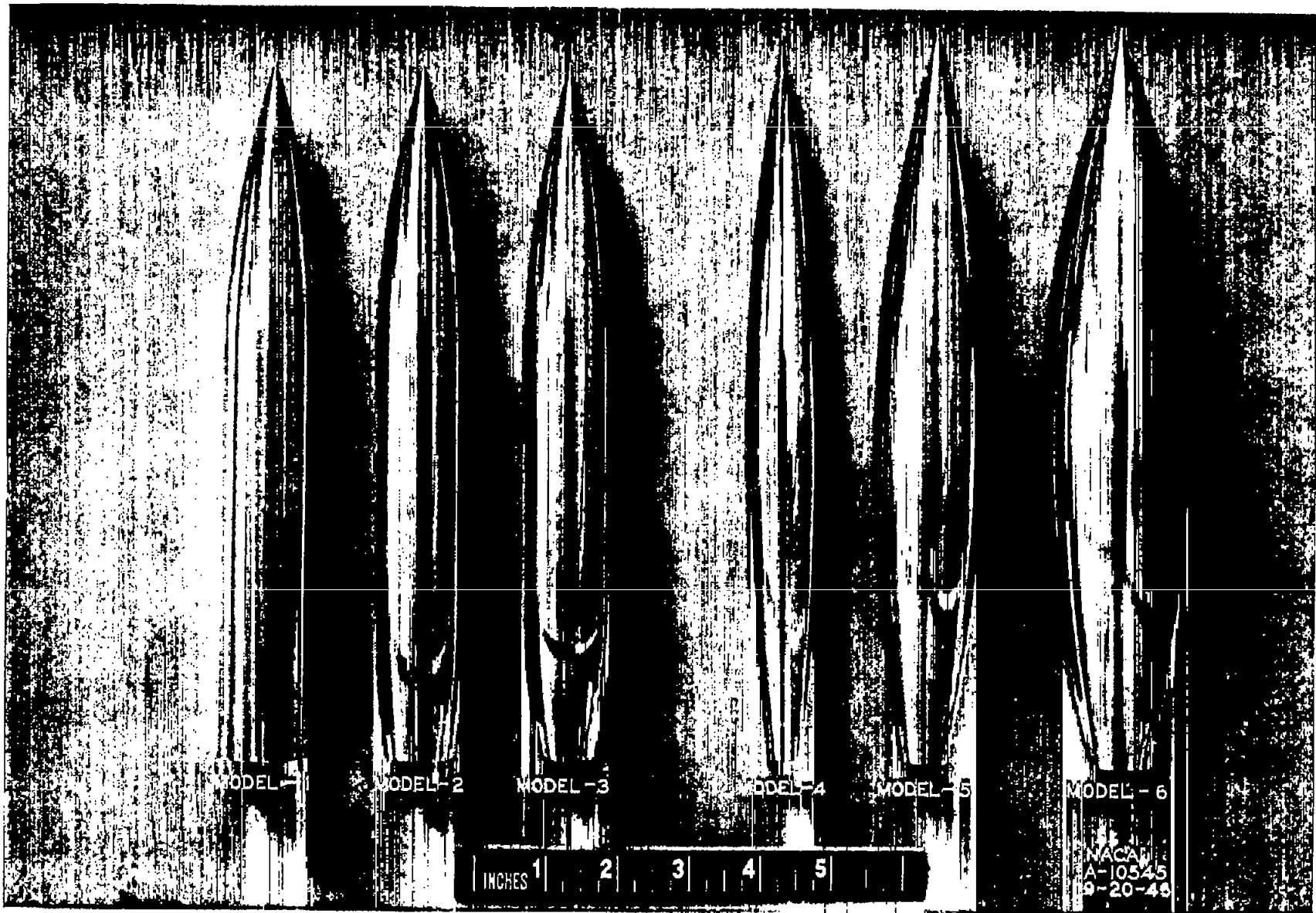
FIGURE 1.—Principal body shapes investigated.
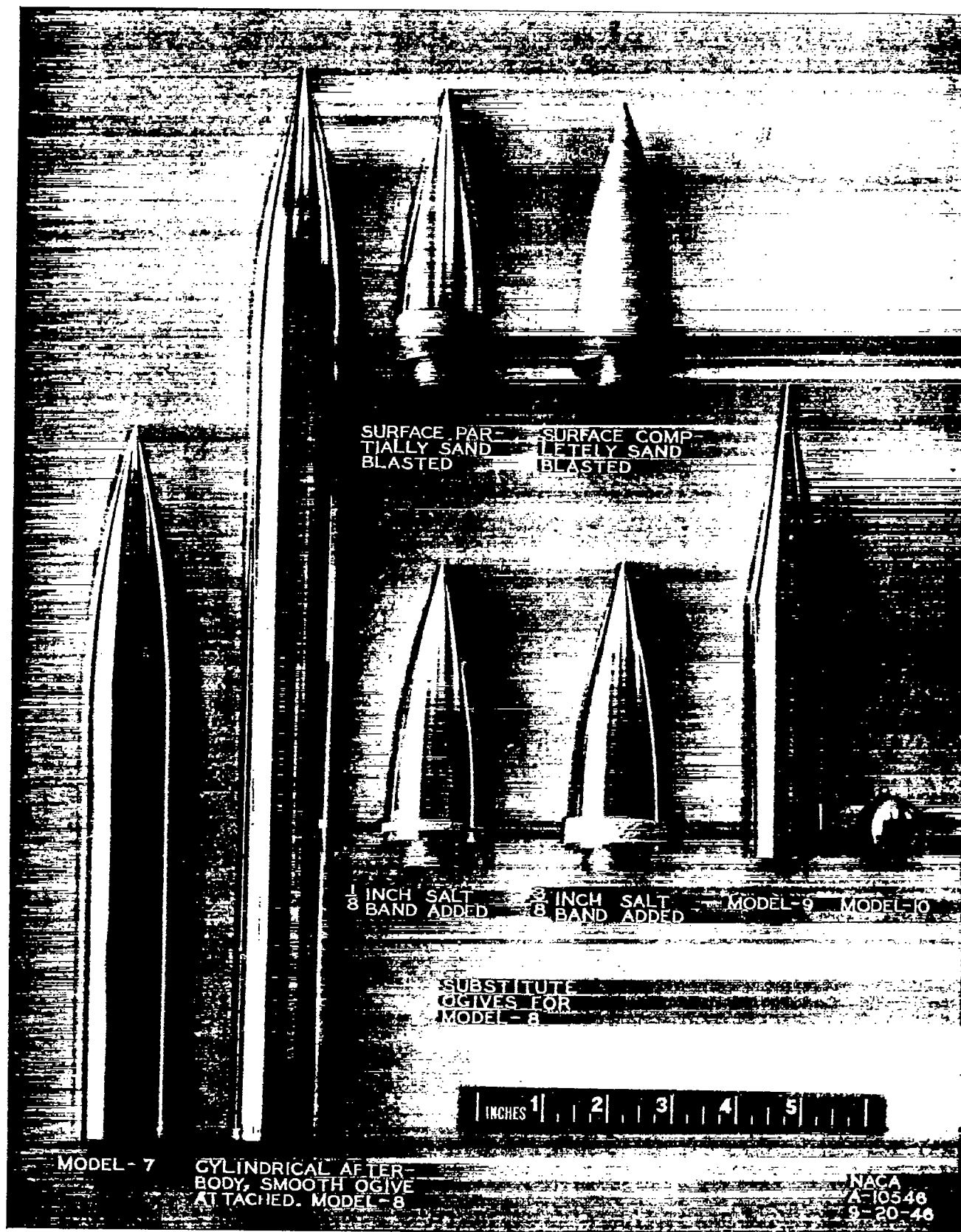
Figure 1

(a) Models used for boundary-layer tests and for comparison tests with other investigations.

FIGURE 2.—Special-purpose models.
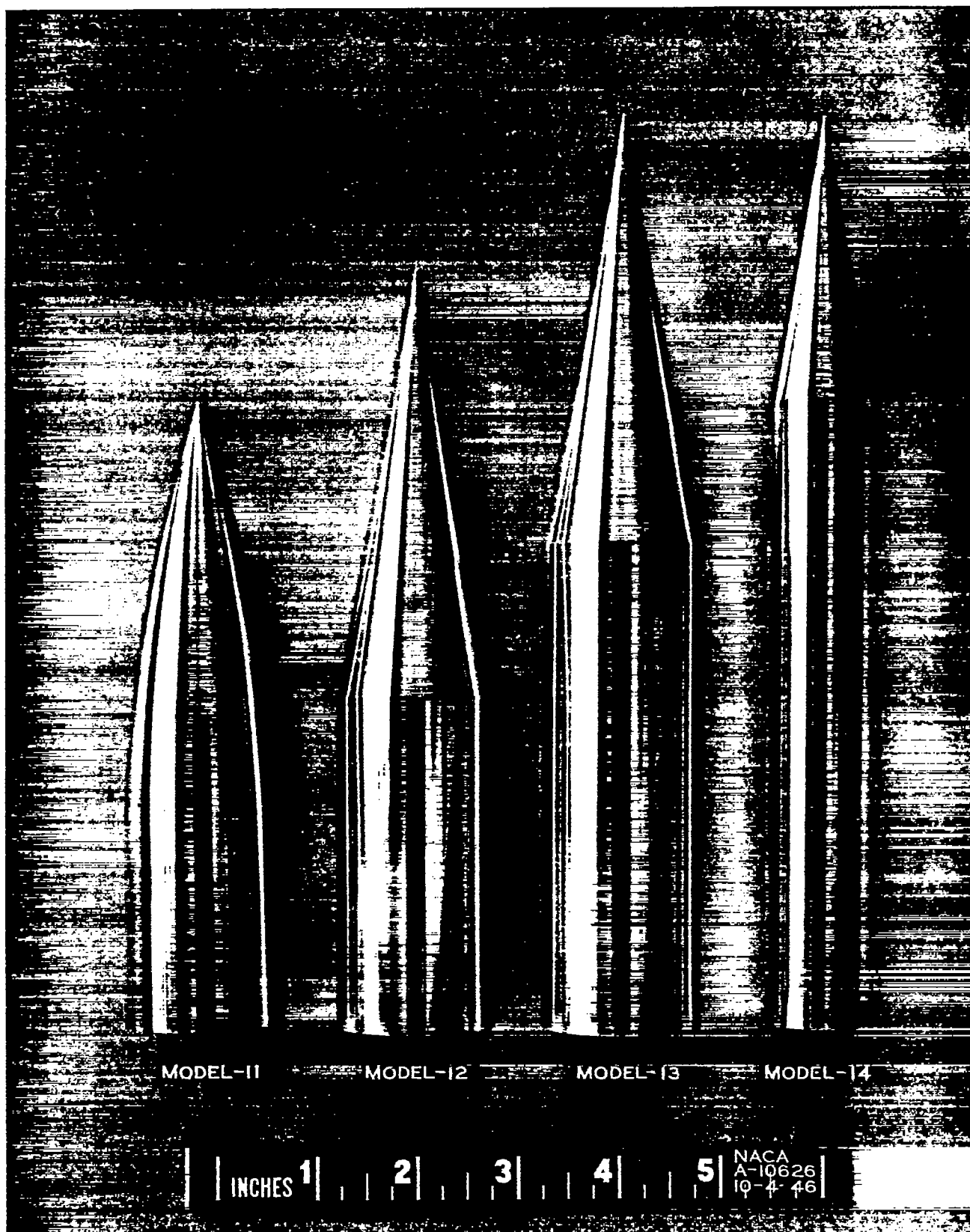
(b) Models used to evaluate effect of length-diameter ratio on base pressure.

FIGURE 2.—Concluded.

CONFIDENTIAL

R=10 D

R=6 D

MODEL 1
MODEL 2
MODEL 3

R=10 D

18.2°

D=1.25

3.12 D

1.97

7 D

R=10 D

18.2°

D=1.50

MODEL 11   8.5
MODEL 7   11.0
MODEL 8   16.7
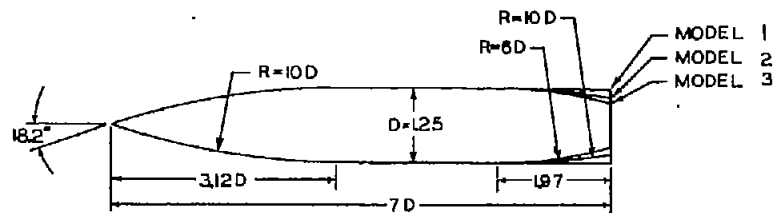
NOTE: ALL DIMENSIONS IN INCHES.
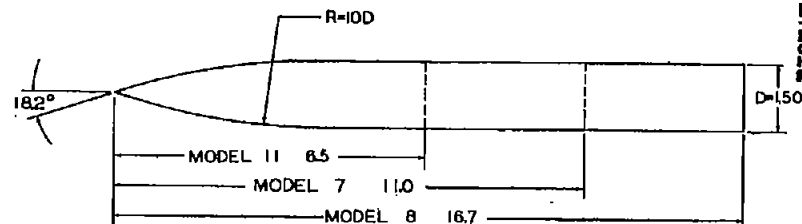
NOTE: ALL DIMENSIONS IN INCHES.

CONFIDENTIAL

9.26

5.25

X

Y

θ

D

CONFIDENTIAL

10°

D

L
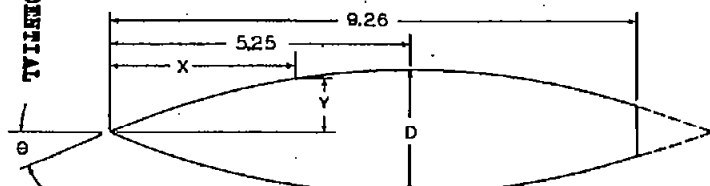
MODEL 4 $Y=2.1\left[\frac{X}{10.5}-\left(\frac{X}{10.5}\right)^{2}\right]$ θ=11.3°   D=1.05

MODEL 5 $Y=3.0\left[\frac{X}{10.5}-\left(\frac{X}{10.5}\right)^{2}\right]$ θ=15.9°   D=1.50

MODEL 6 $Y=4.2\left[\frac{X}{10.5}-\left(\frac{X}{10.5}\right)^{2}\right]$ θ=21.8°   D=2.10

MODEL 9   L=7.5   D=1.25
MODEL 10   SPHERE   D=1.00
MODEL 12   L=7.5   D=1.50
MODEL 13   L=9.0   D=1.50
MODEL 14   L=9.0   D=1.00

NACA
A-10824
11-7-46

(b) MODELS WITH CYLINDRICAL AFTERBODIES.

(a) BOAT-TAILED BODIES.

NACA
A-10825
11-7-46

FIGURE 3 - MODEL DIMENSIONS.

FIGURE 3 - CONCLUDED.

Fig. 3

DRAG GAGE

STING

SHROUD

L. M. MASTIN

NACA
A-10584
10-1-46
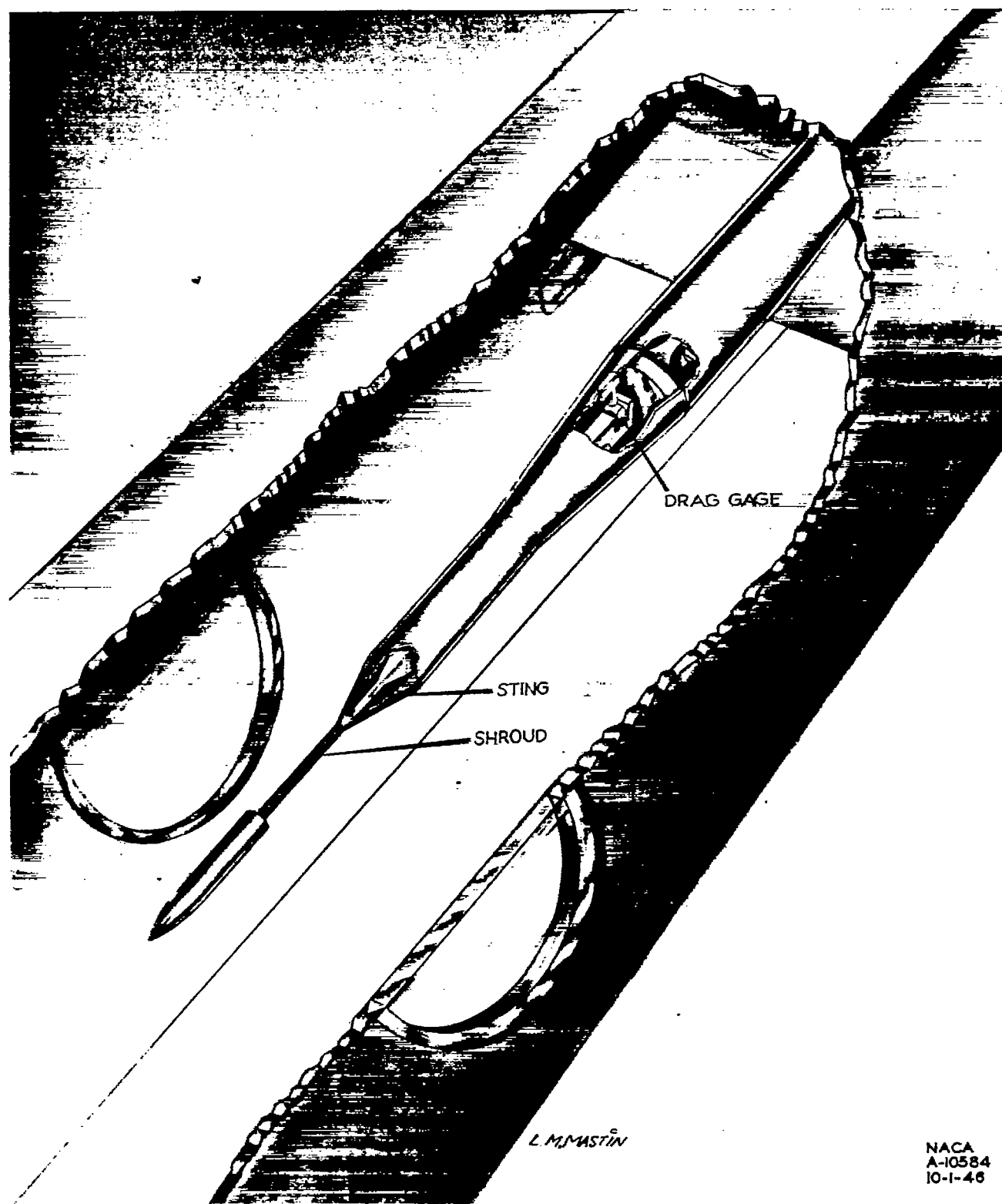
FIGURE 4.—Schematic diagram of model installation with rear support and drag gage.

SLIDING BEAM

L.M.NASTIN

NACA
A-10585
10-1-46
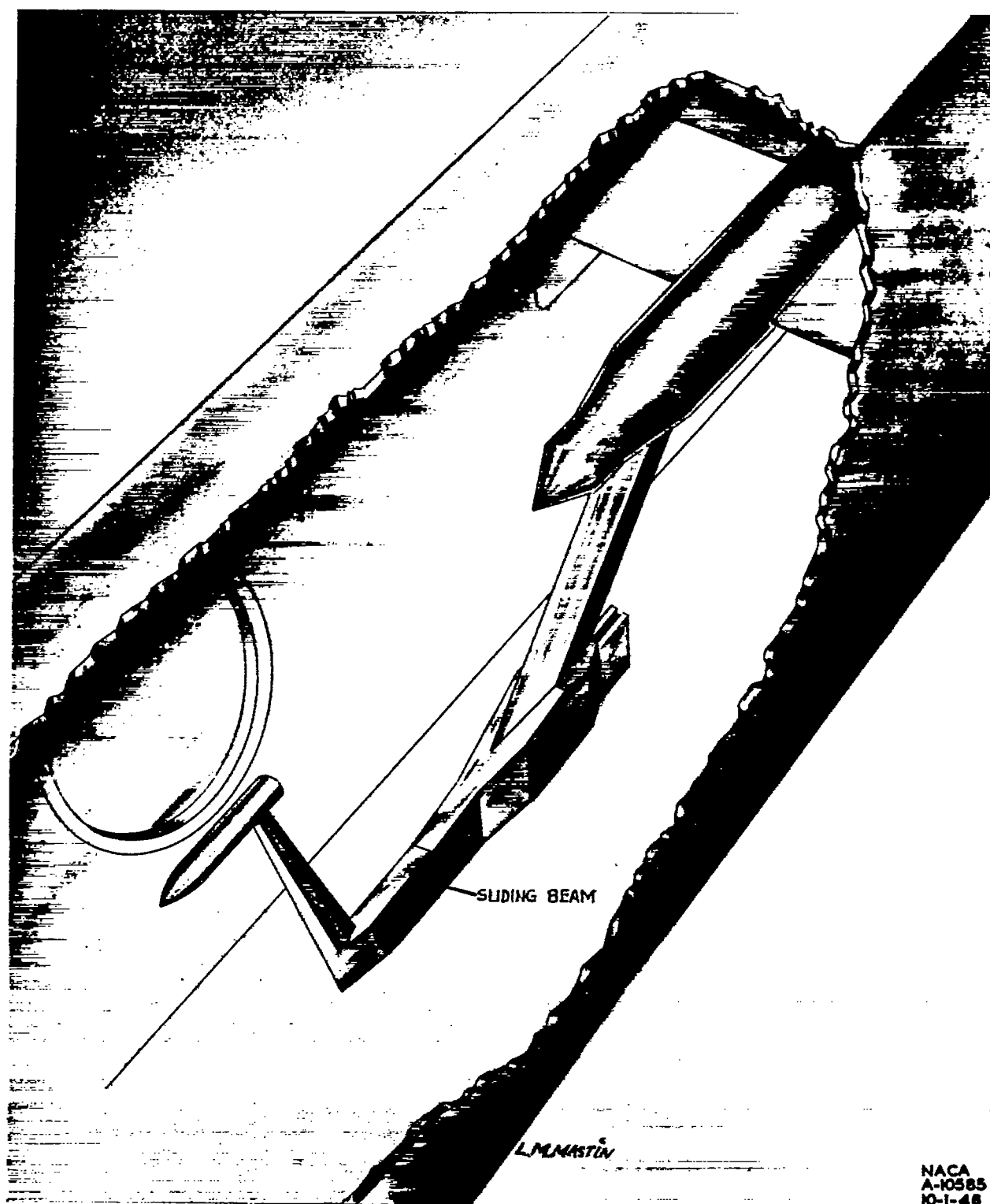
FIGURE 5.—Schematic diagram of model installed with side support.
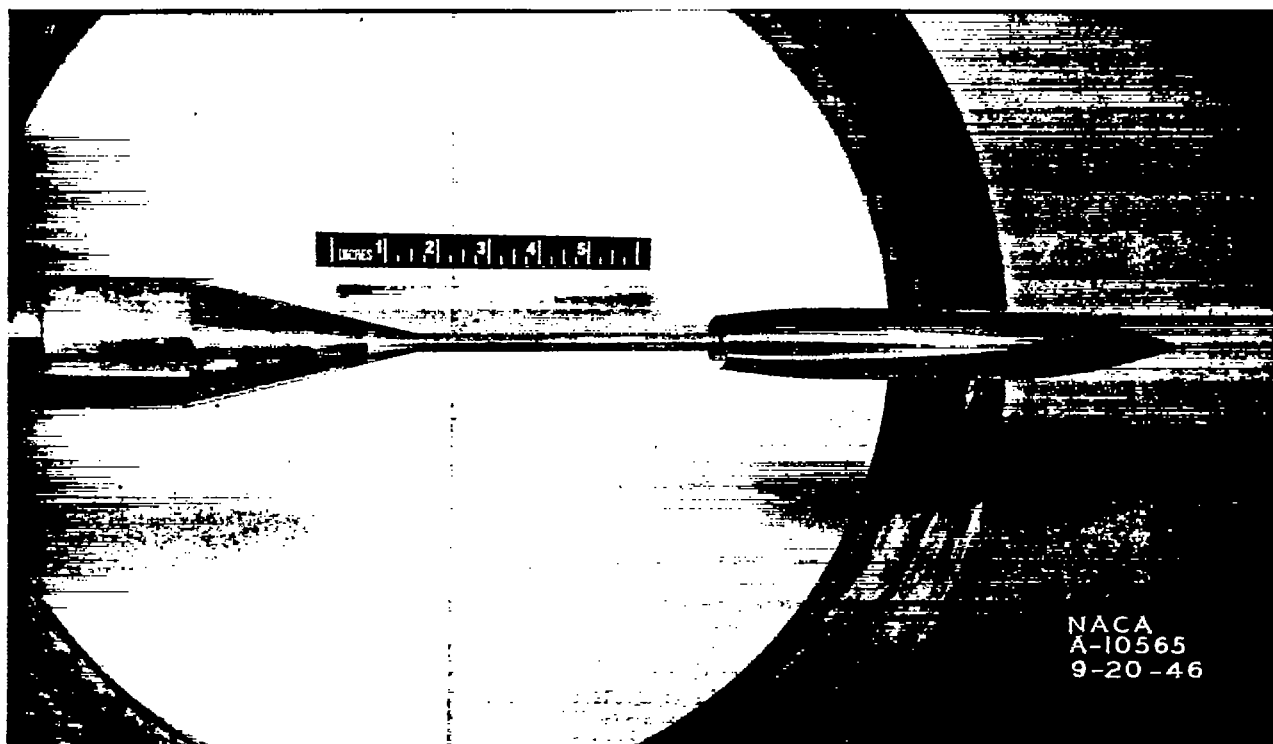
(a) Rear support.
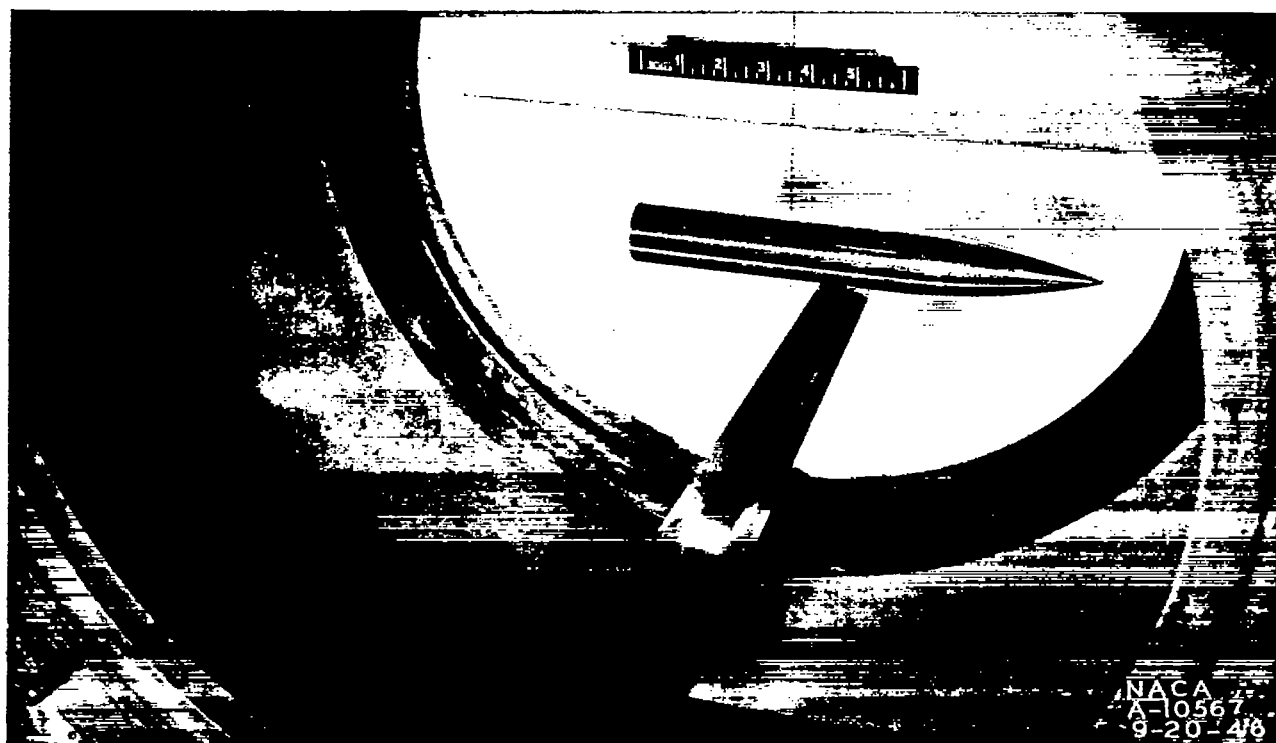
(b) Side support.

FIGURE 6.—Typical model installations.
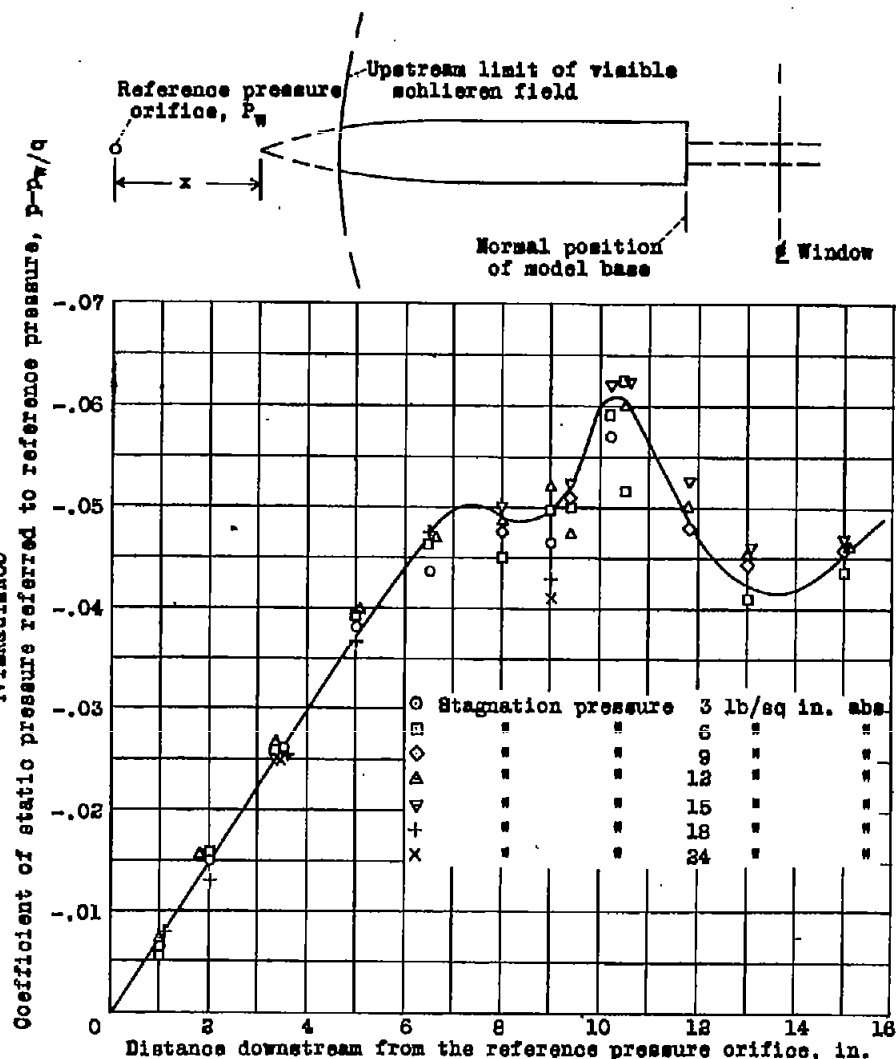
Figure 7.- Axial variation of the static pressure in the test section of the M = 1.5 nozzle.
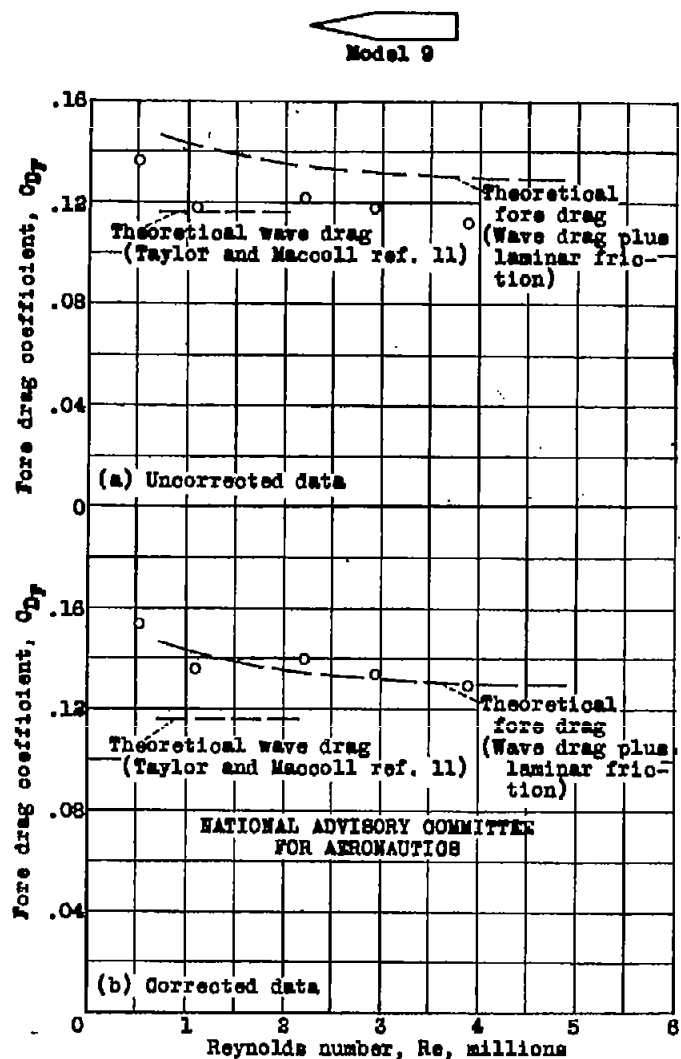
Model 9

Figure 8.- Comparison of fore drag coefficients of model 9 with and without corrections applied for the axial variation of test-section static pressure.

CONFIDENTIAL Fig. 9

Model 1

(See figure 7 for definition of x)

(a) Uncorrected data

O x = 0 in.
□ x = 1.3 in.
◇ x = 2.4 in.
△ x = 3.8 in.
▽ x = 5.0 in.

NATIONAL ADVISORY COMMITTEE
FOR AERONAUTICS

(b) Corrected data

Reynolds number, Re, millions
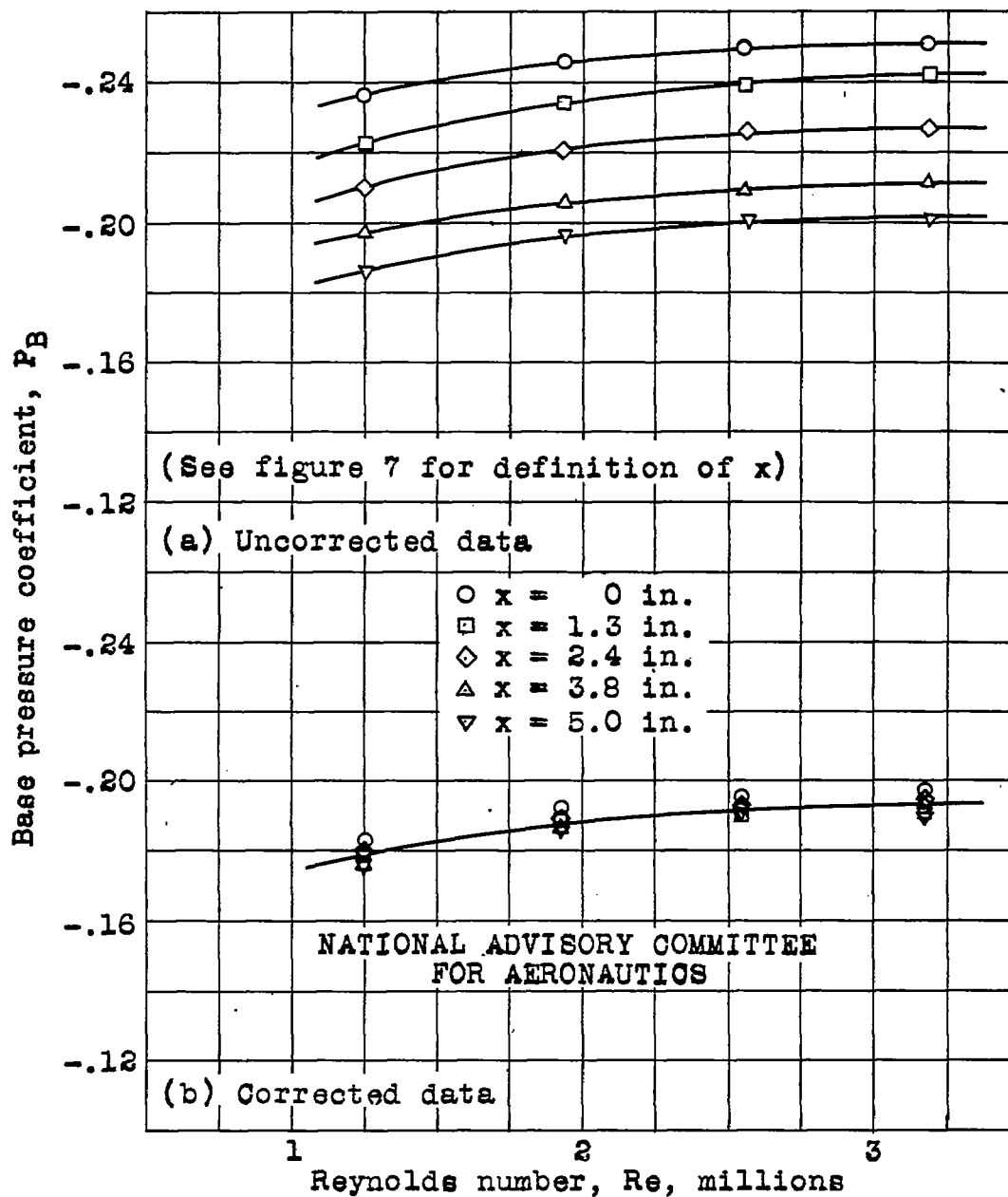
Figure 9.— Comparison of base pressure coefficients on
model 1 measured at various positions along
the tunnel axis, with and without corrections applied
for the variation of test-section static pressure.
CONFIDENTIAL

LINE OF INTERSECTION OF
CONICAL SHOCK WAVE
AND GLASS SIDE WALLS

CONICAL SHOCK WAVE
ON NOSE OF MODEL

SHOCK WAVE
ON NOSE OF
MODEL SUPPORT

MODEL SUPPORT

TURBULENT WAKE
BEHIND MODEL

SHOCK WAVES
ORIGINATING FROM
TUNNEL WALLS

TRAILING SHOCK WAVE
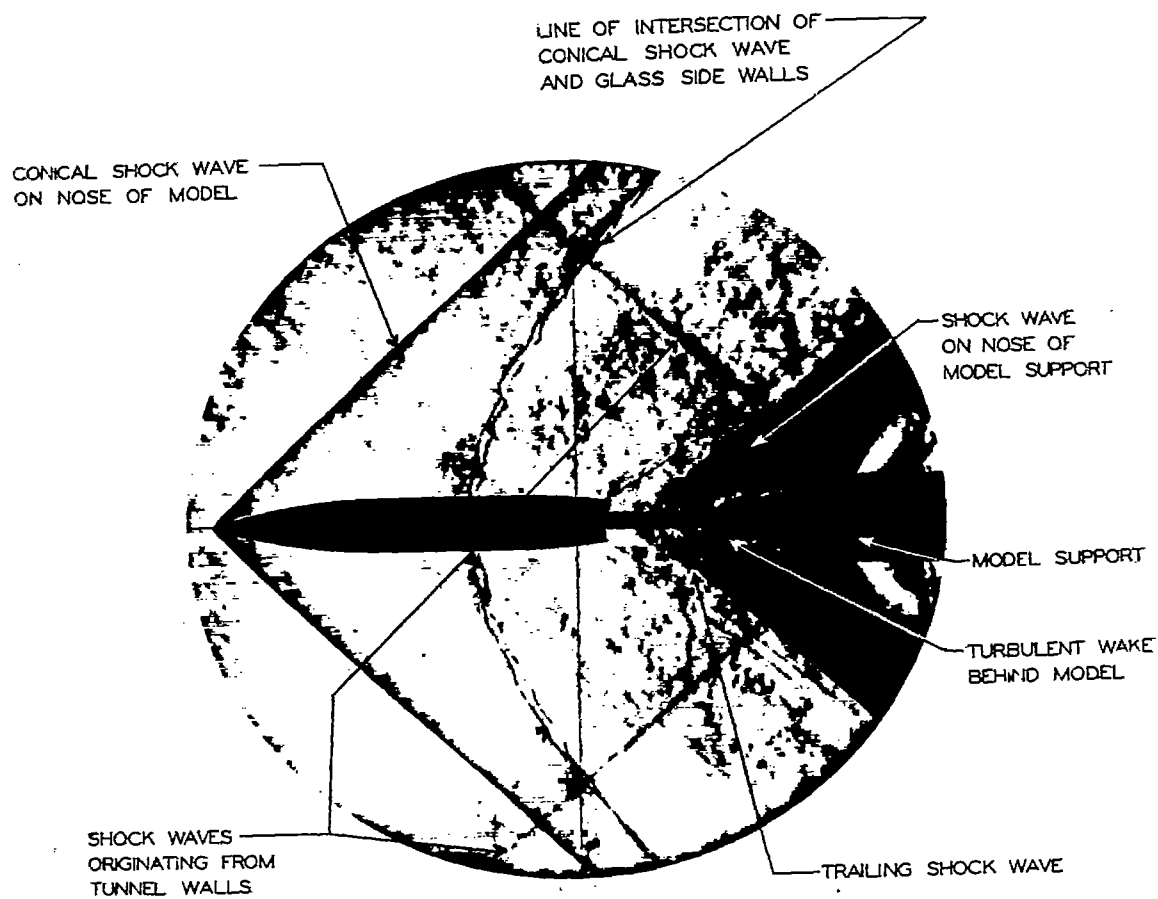
NACA
A-9224
1-14-46

FIGURE 10.—Typical schlieren photograph.

CONFIDENTIAL

CONFIDENTIAL

SHOCK WAVE

36.4° ANGLE BETWEEN
SURFACE TANGENTS
AT THE NOSE.

MACH NET – MODEL 3

VALUE GIVEN BY TAYLOR & MACCOLL
FOR AN 18.2° CONE, REFERENCE 10.

NATIONAL ADVISORY COMMITTEE
FOR AERONAUTICS

LINEAR THEORY, REFERENCE 13.

METHOD OF CHARACTERISTICS, REFERENCE 12.

.32

.24

.16

.08

0

-.08

-.16

PRESSURE COEFFICIENT, $\dfrac{P-P_i}{q_i}$

PRESSURE DISTRIBUTION   M = 1.5
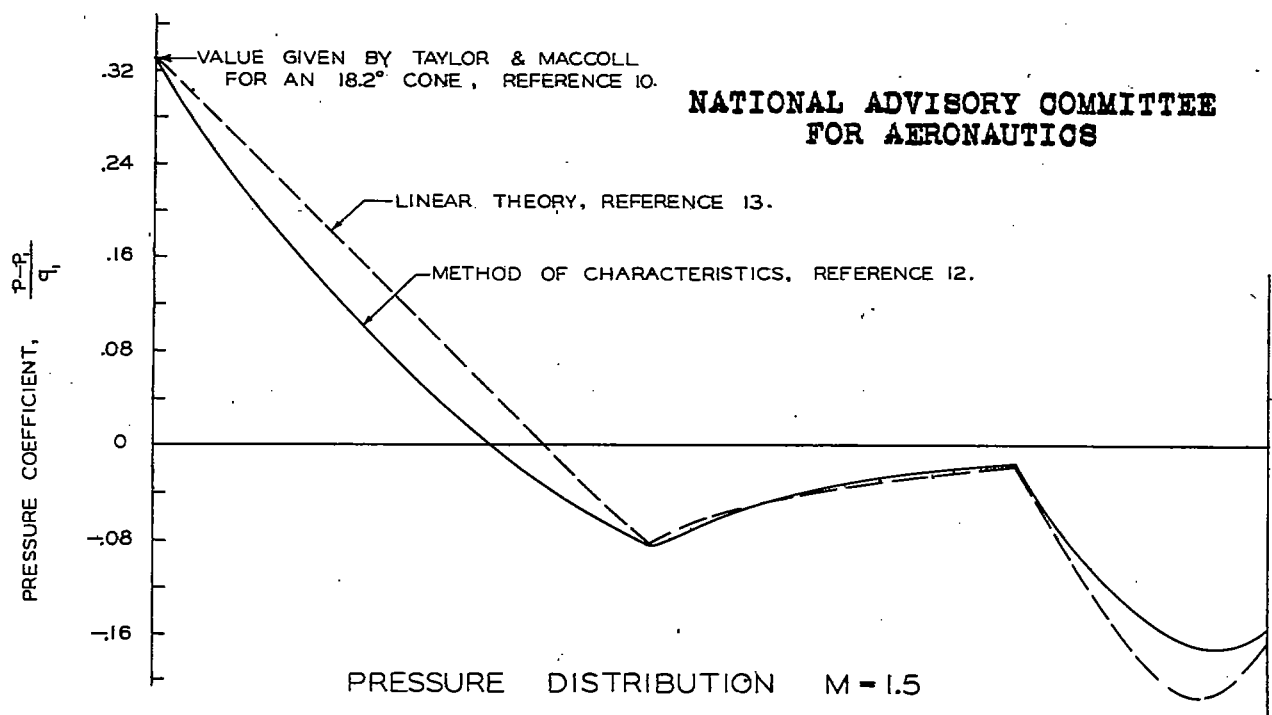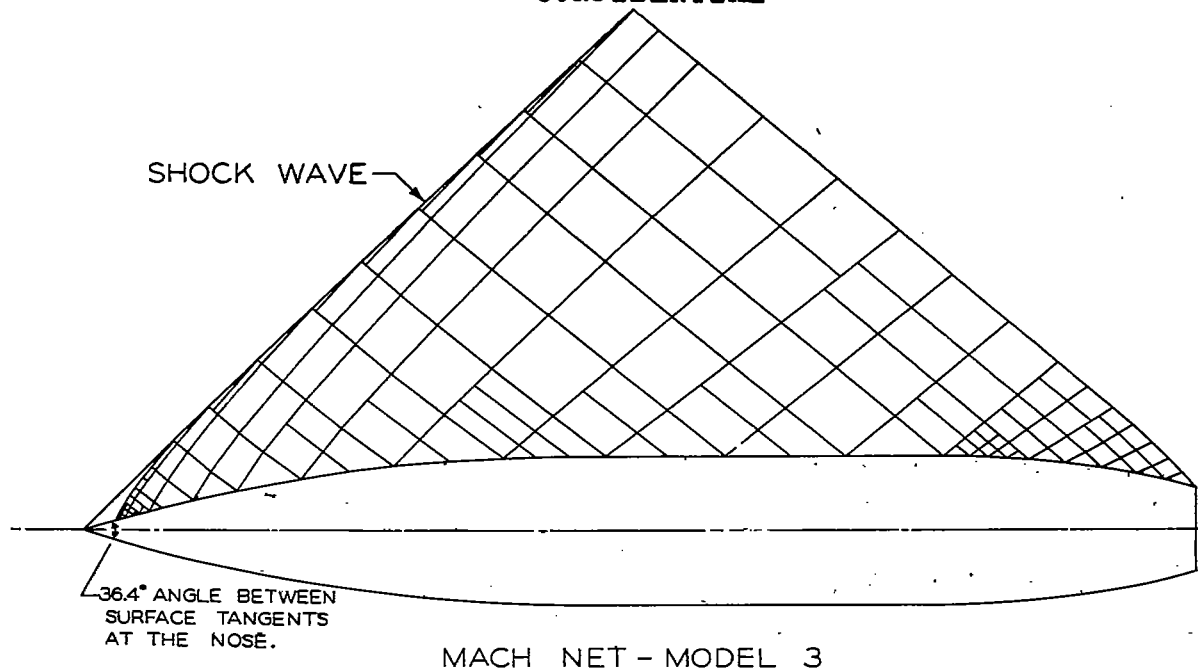
FIGURE 11. – TYPICAL MACH NET AND PRESSURE DISTRIBUTION
FOR THE FLOW OVER A BOAT TAILED BODY.

CONFIDENTIAL
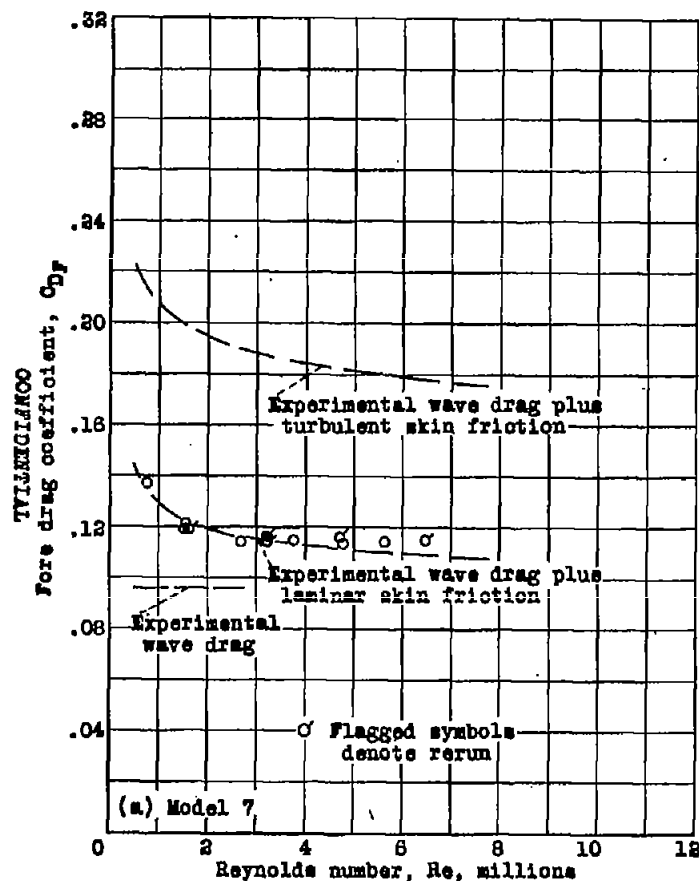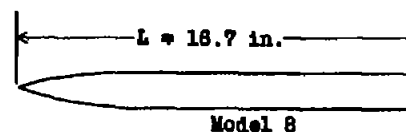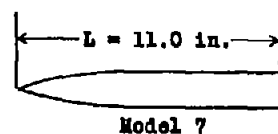
NACA
A-10683
10-21-46

Figure 13.- Variation of fore drag coefficient with Reynolds number for models with long cylindrical afterbodies.

Figure 13.- Concluded.

Fig. 13

Re=3.7 x 10⁶.

Re=6.5 x 10⁶.
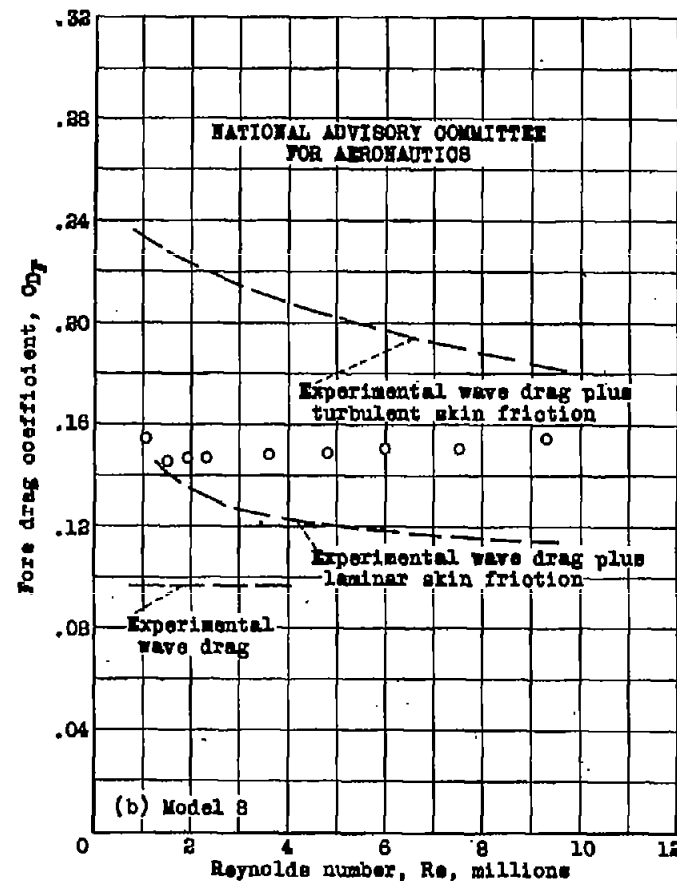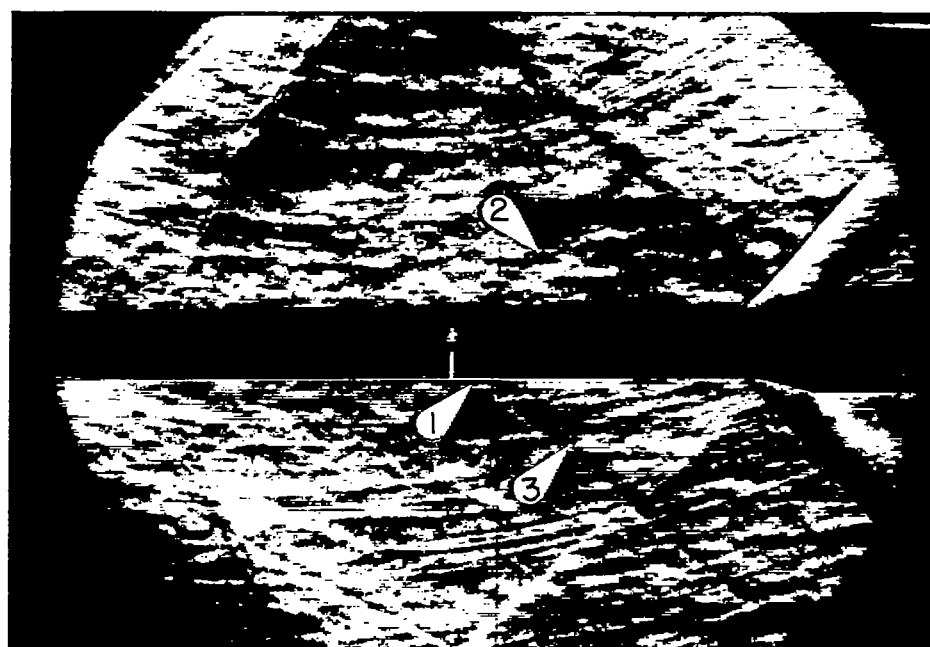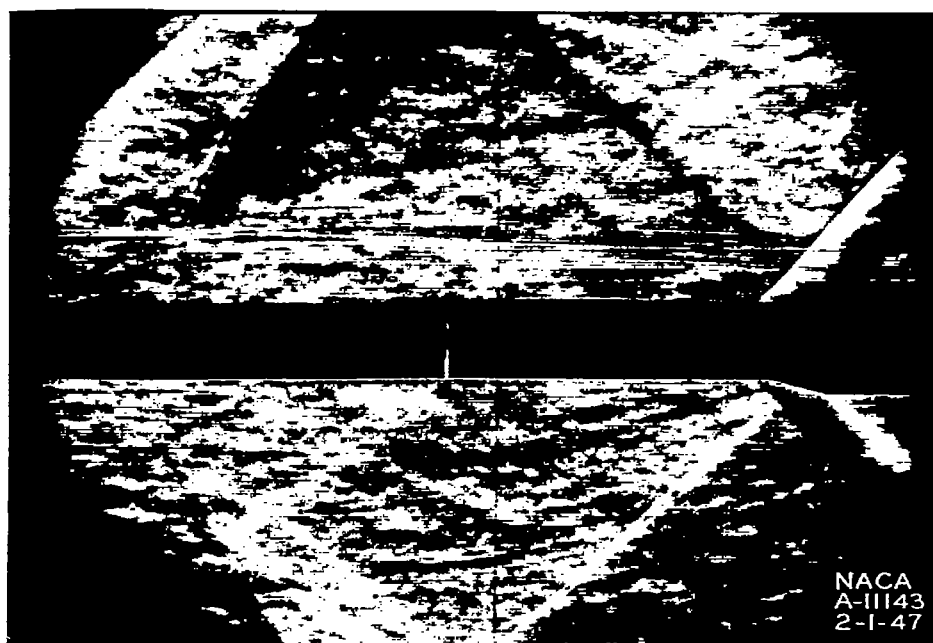
FIGURE 13.—Schlieren photographs showing laminar flow over the cylindrical afterbody of model 7 at two values of the Reynolds number. Knife edge horizontal.

CONFIDENTIAL
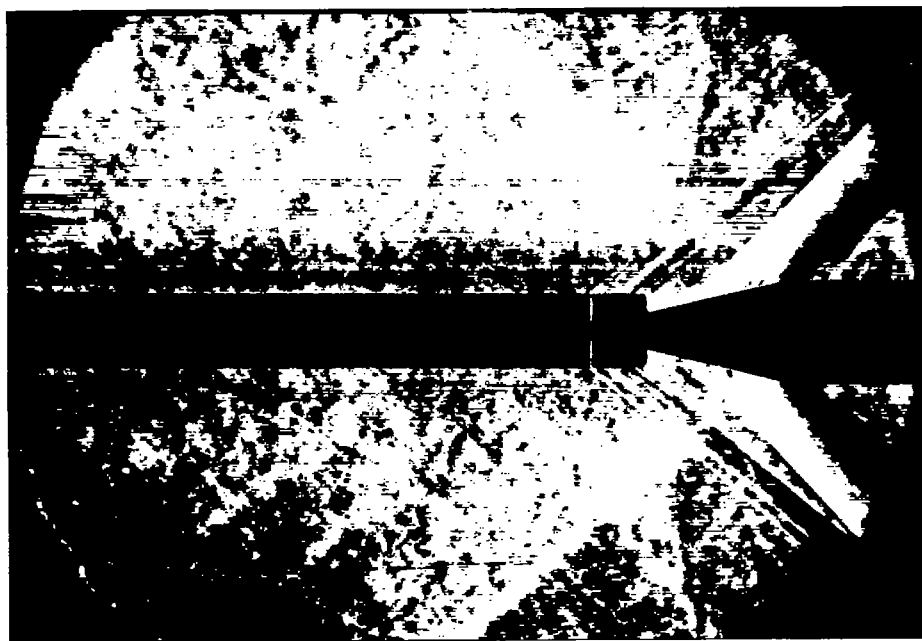
(a) Knife edge vertical.
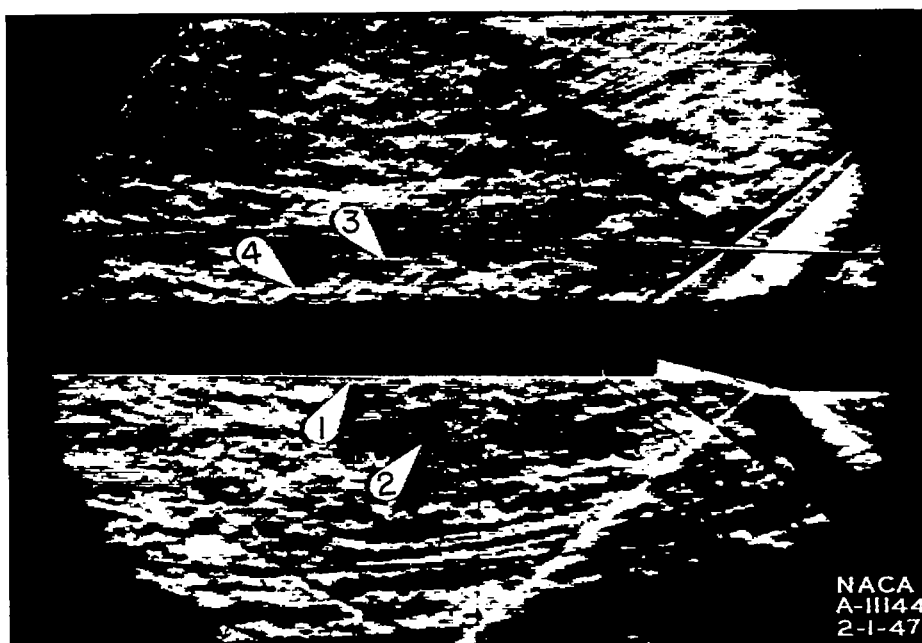
(b) Knife edge horizontal.

FIGURE 14.—Schlieren photograph showing premature transition on the cylinder afterbody of model 8. Reynolds number 9.35 million.

CONFIDENTIAL

Theoretical pressure distribution, free flight

Theoretical pressure distribution with the
effect of tunnel static pressure gradient
included for x = 1.5.
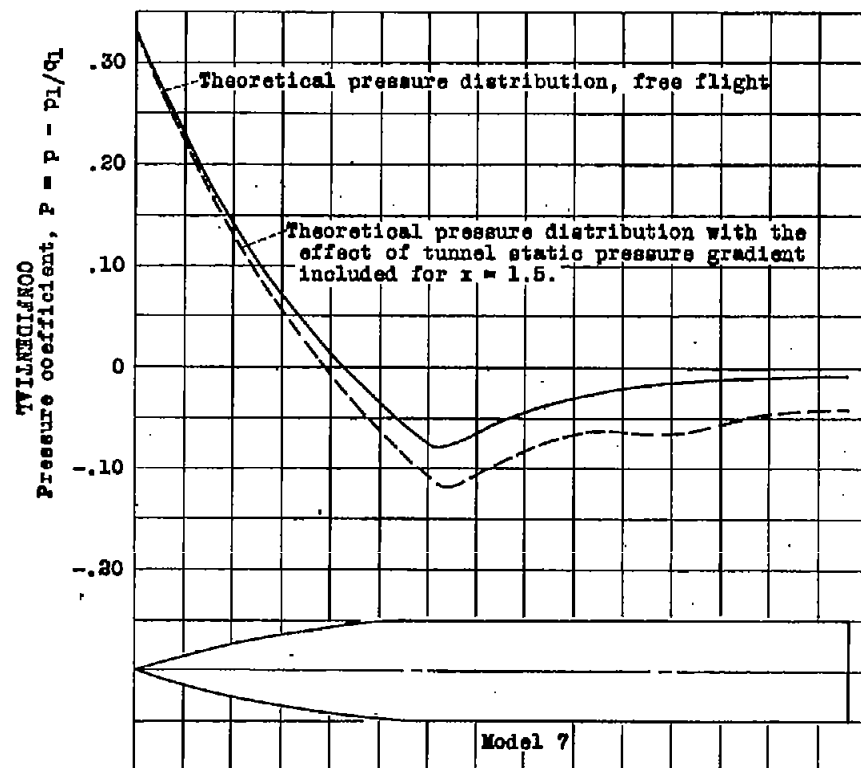
Model 7

Figure 15.- Theoretical pressure distribution over the
surface of model 7 at zero angle of attack and
1.5 Mach number.

Roughness added

Shroud

NATIONAL ADVISORY COMMITTEE
FOR AERONAUTICS

O Complete sand blast
□ 3/8 inch salt band
◇ 3/16 inch salt band
△ 1/8 inch salt band
▽ Smooth surface

Reynolds number, Re, millions
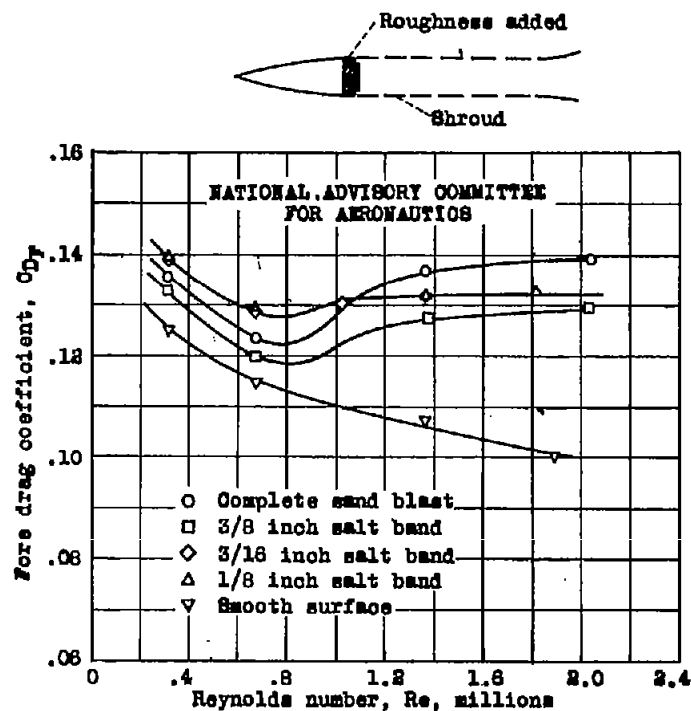
Figure 16.- Variation of fore drag coefficient
with Reynolds number of the ogives
with varying degrees of roughness added.

CONFIDENTIAL
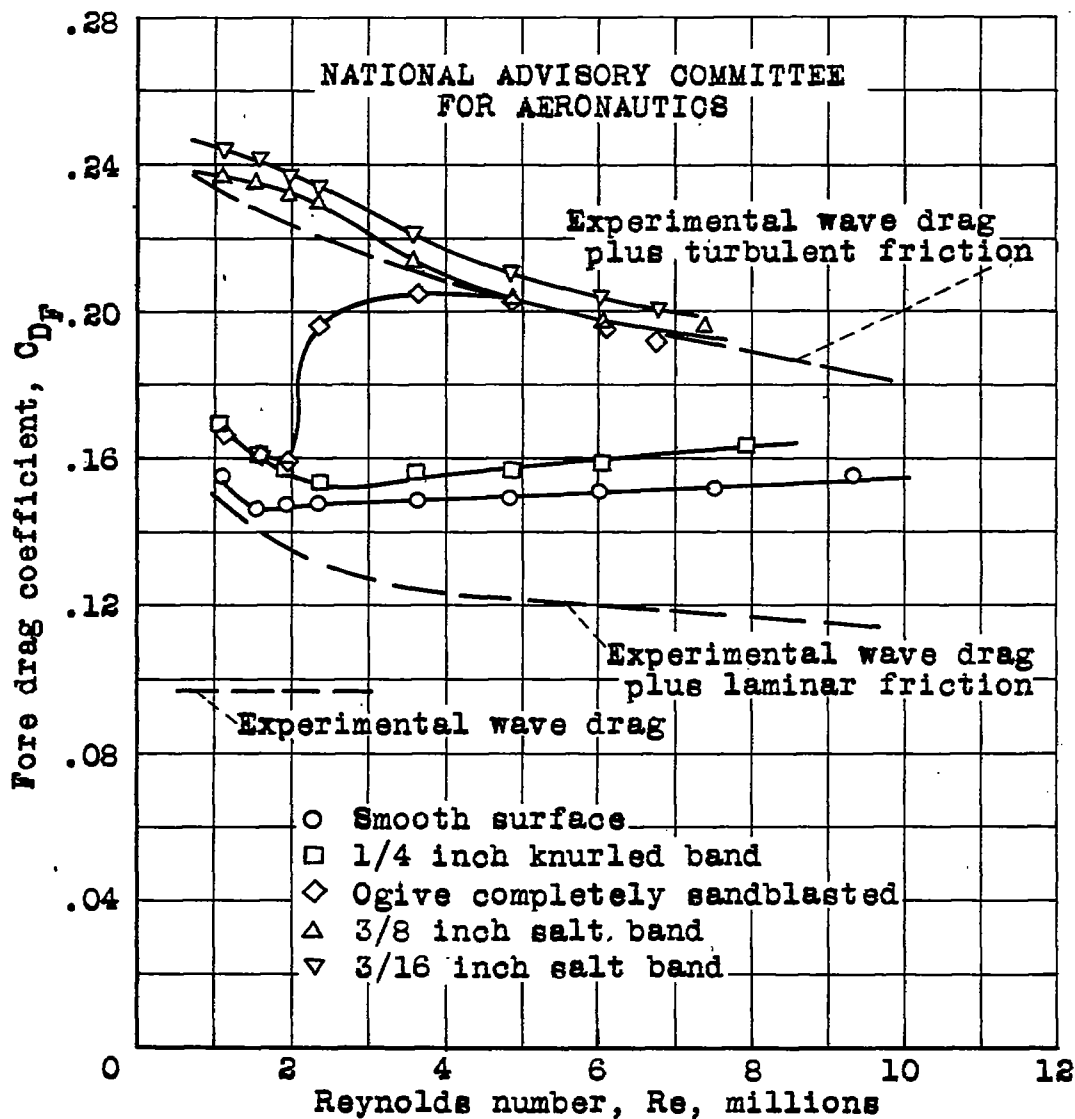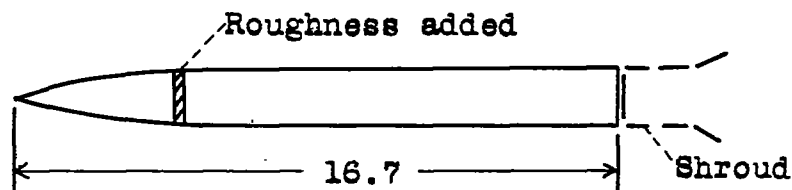
Figure 17.- Variation of fore drag coefficient
with Reynolds number for model 8
with various amounts of roughness.

CONFIDENTIAL
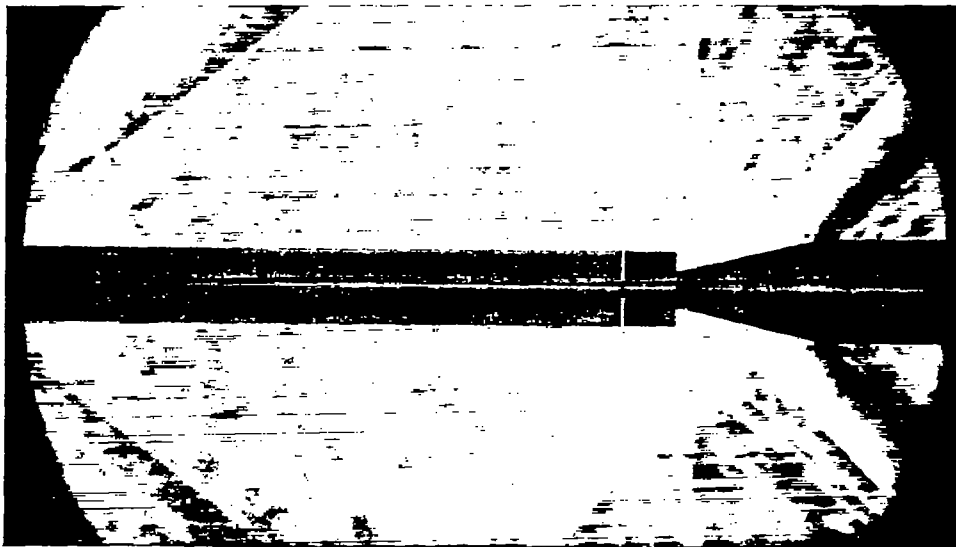
(a) Knife edge vertical.
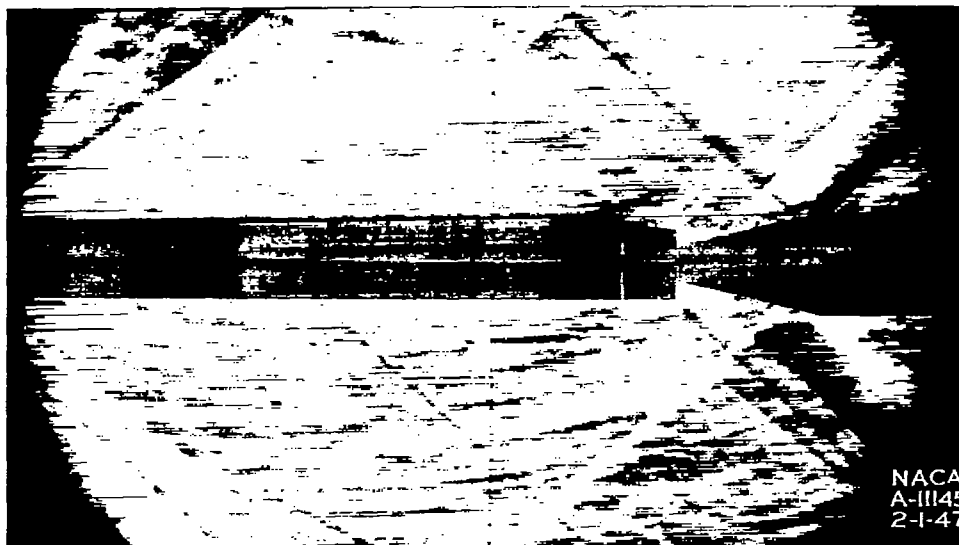
(b) Knife edge horizontal.

FIGURE 18.—Schlieren photographs of model 8 with transition fixed. Reynolds number 7.2 million.

CONFIDENTIAL

Re=0.58 x 10⁶.

Re=0.87 x 10⁶.

Re=1.1 x 10⁶.
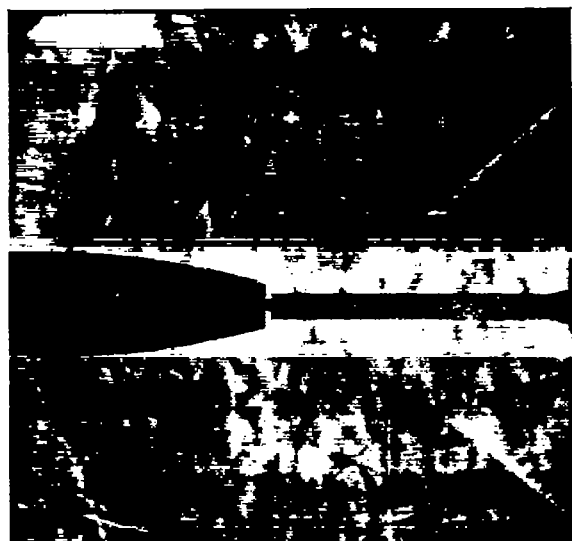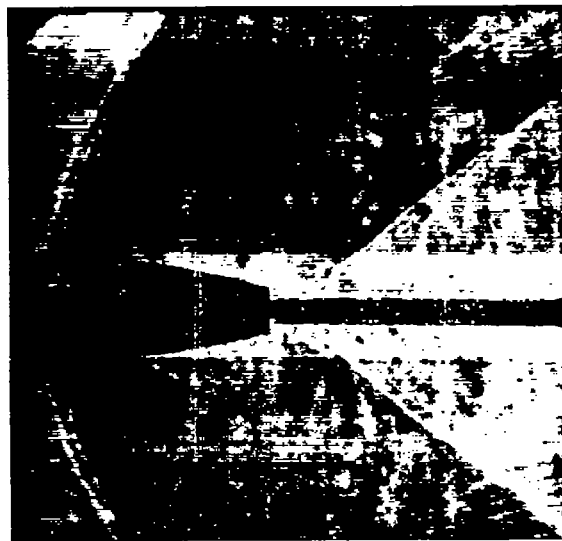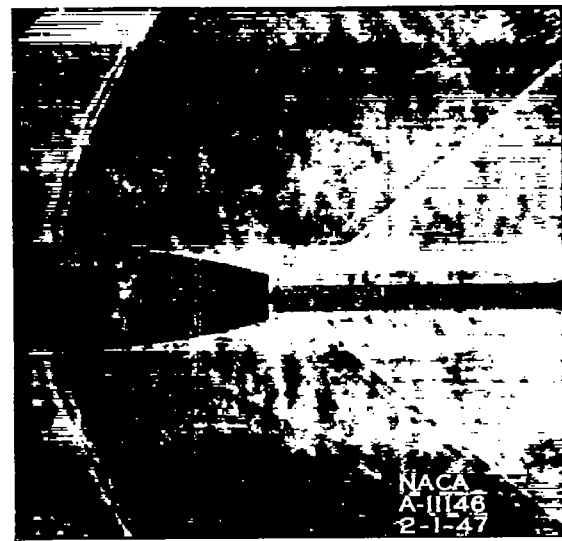
Re=1.4 x 10⁶.

FIGURE 19.—Schlieren photographs showing the effect of Reynolds number on laminar separation for model 6. Knife edge vertical.

Re=0.79 x 10⁶.   Re=3.8 x 10⁶.

Model 2

Re=1.2 x 10⁶.   Re=3.8 x 10⁶.
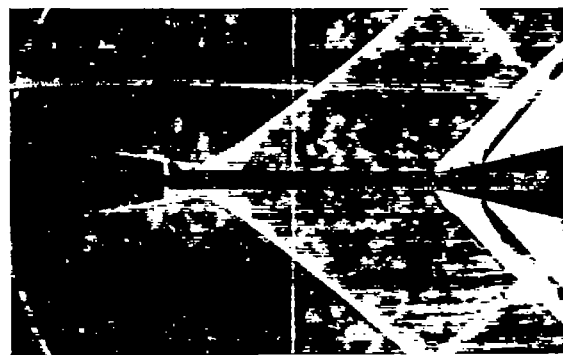
Model 3

Re=0.10 x 10⁶.   Re=0.45 x 10⁶.

Model 10

FIGURE 20.—Schlieren photographs showing the effect of Reynolds number on laminar separation for models 2, 3, and 10.   Knife edge vertical.

CONFIDENTIAL
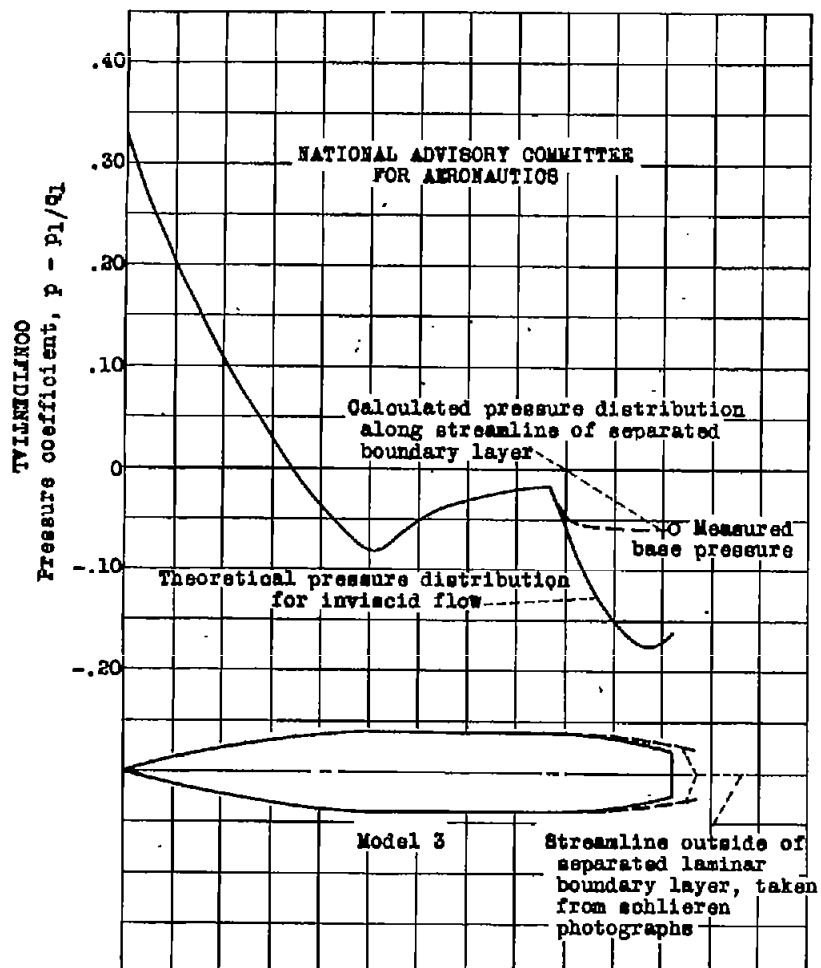
Figure 21.— Calculated pressure distribution for model 3 at 0.6 million Reynolds number.
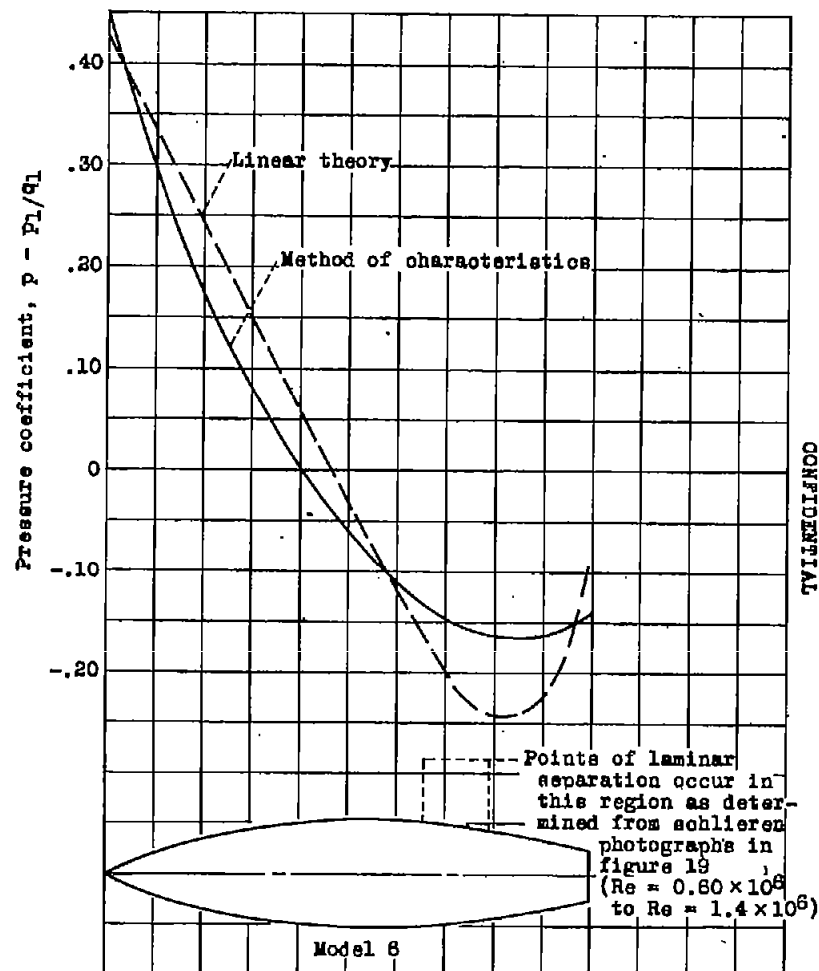
Figure 22.— Calculated pressure distribution on model 6.
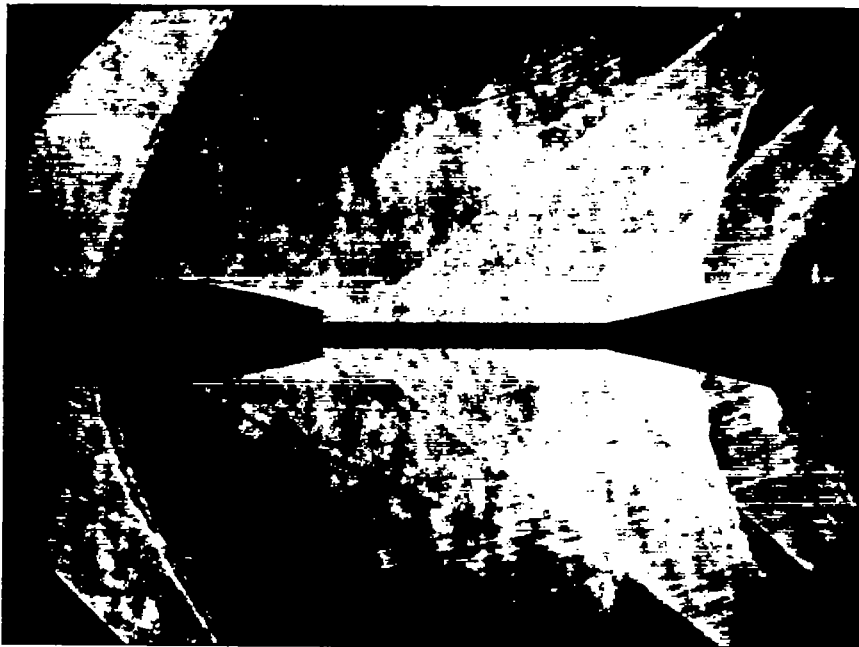
(a) Laminar boundary layer, Re=0.87 x 10⁶.
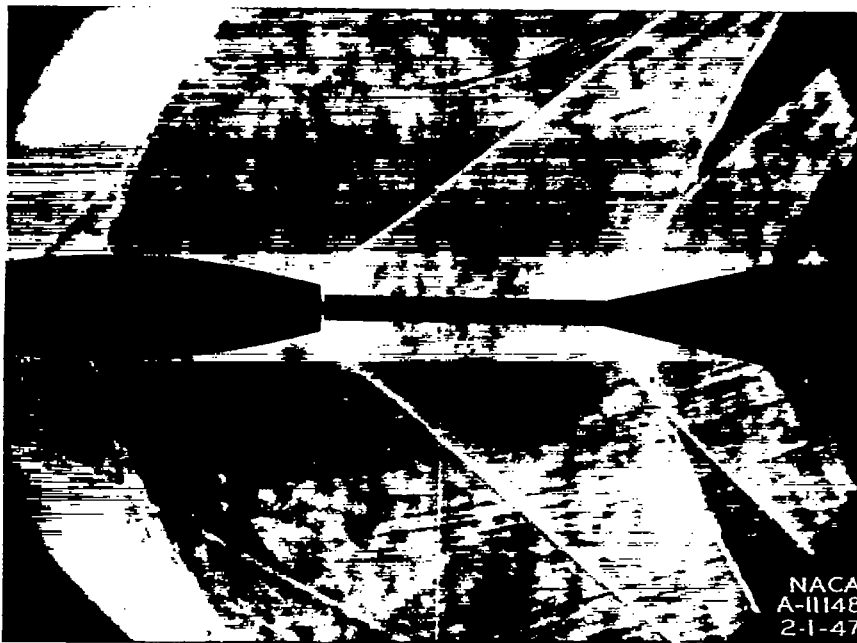
(b) Turbulent boundary layer, Re=0.87 x 10⁶.

FIGURE 23.—Schlieren photographs of model 6 illustrating the effect on flow separation of the condition of the boundary layer.

CONFIDENTIAL

CONFIDENTIAL

Figure 24

Model 1
Re=3.8 x 10⁶.
$\beta=0°.$

Model 4
Re=4.0 x 10⁶.
$\beta=8.55°.$
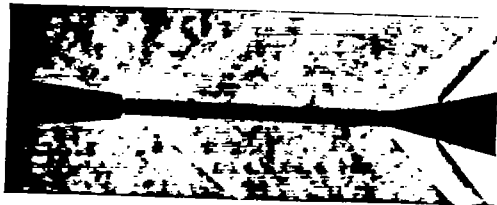
Model 2
Re=3.8 x 10⁶.
$\beta=9.08°.$

Model 5
Re=2.7 x 10⁶.
$\beta=12.13°.$

Model 3
Re=3.8 x 10⁶.
$\beta=15.25°.$

Model 6
Re=1.1 x 10⁶.
$\beta=16.75°.$
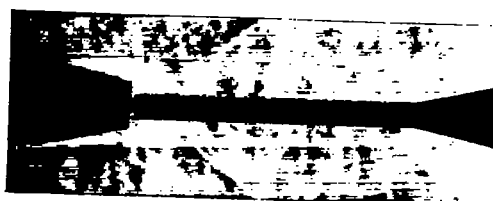
Laminar.

Turbulent.

FIGURE 24.—Schlieren photographs showing the effect of turbulent boundary layer on shock-wave configuration at base of models 1, 2, 3, 4, 5, and 6.   Knife edge vertical.

CONFIDENTIAL

Re=1.2 x 10⁶.

Re=2.6 x 10⁶.

Re=3.9 x 10⁶.
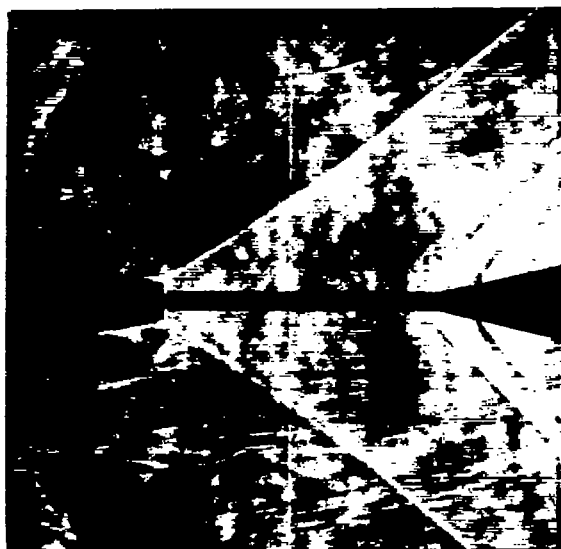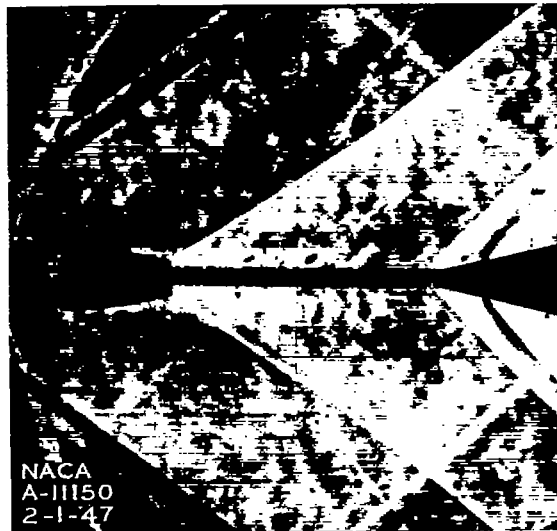
Re=5.1 x 10⁶.

FIGURE 25.—Schlieren photographs showing the absence of any effect of Reynolds number on the flow over the afterbody of model 3 with roughness added. Knife edge vertical.
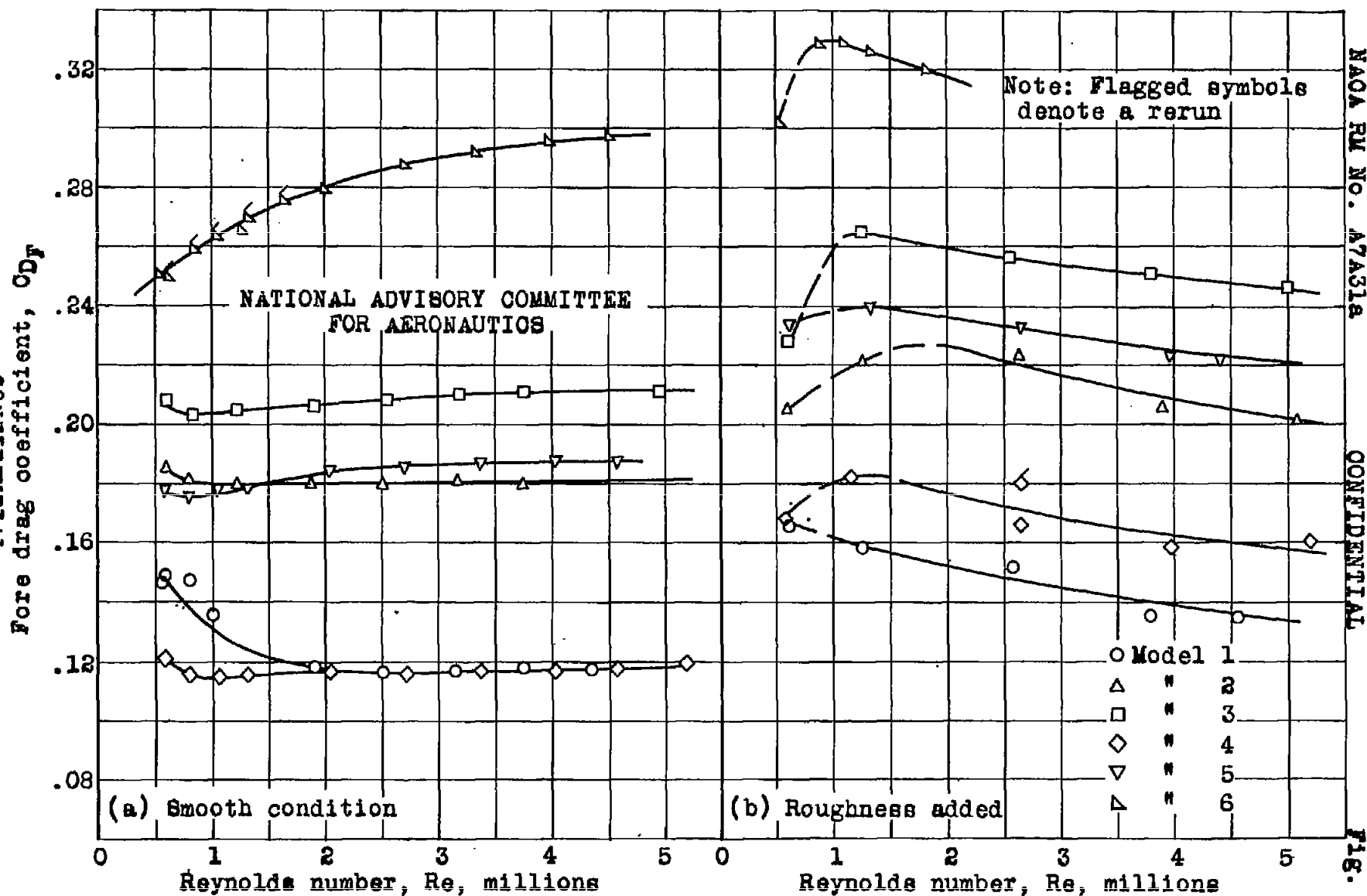
CONFIDENTIAL

Figure 26.– Variation of fore drag coefficient for models 1, 2, 3, 4, 5, and 6 in the smooth condition and with roughness added.
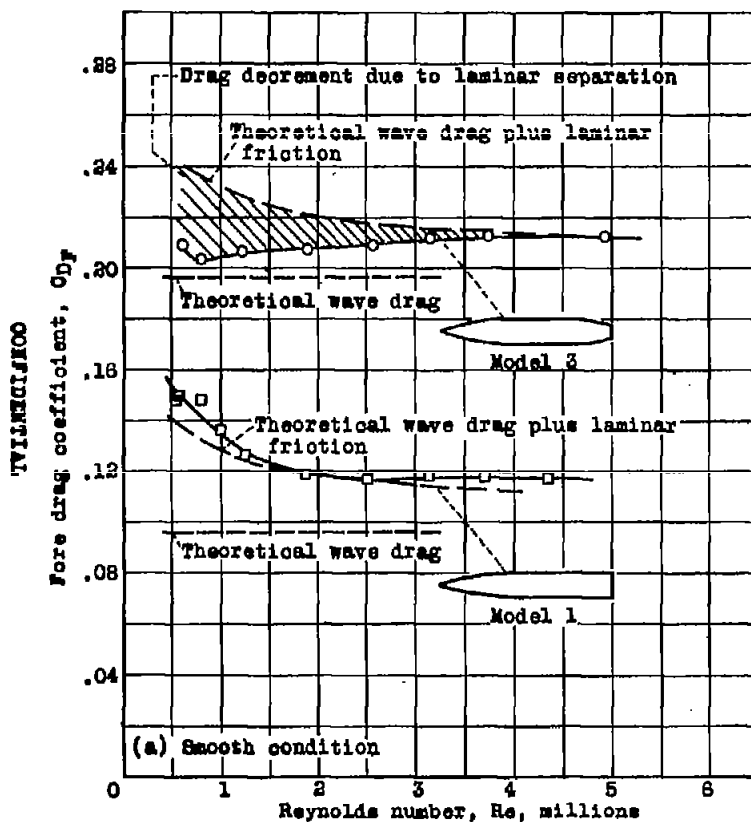
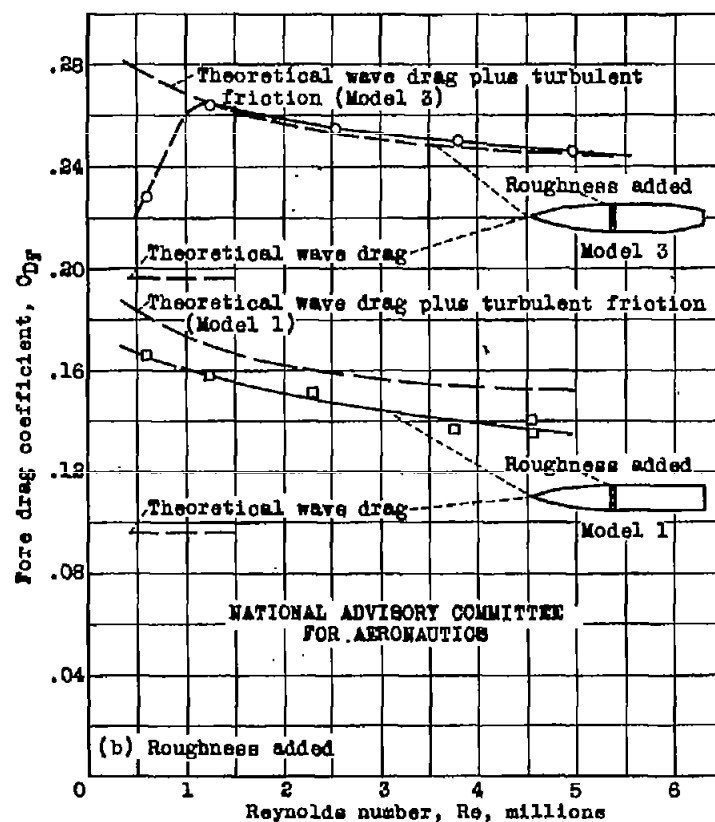Figure 27.- Comparison of theoretical and experimental fore drag coefficients for models 1 and 3.
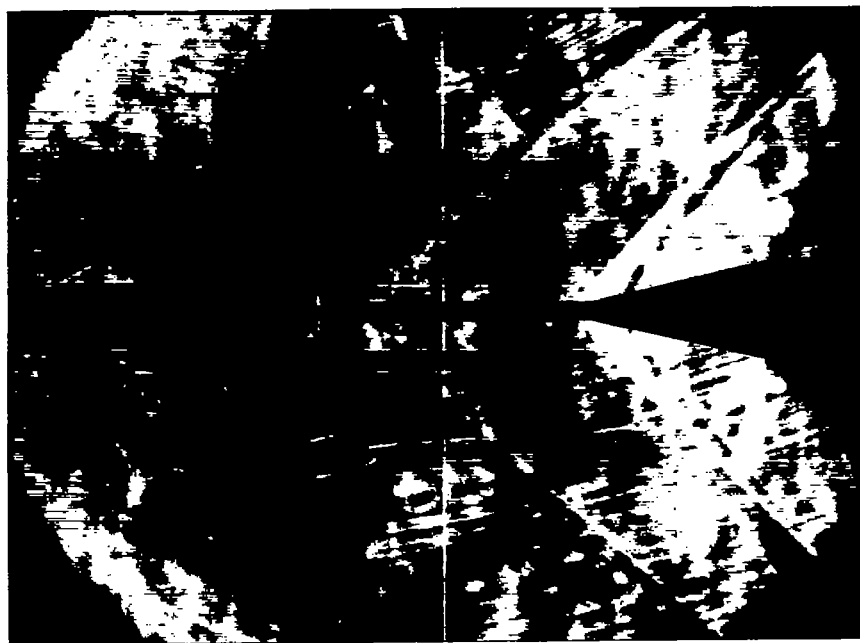
Figure 27.- Concluded.

Fig. 27

Model 3, Re=0.58 x 10⁶.

Model 6, Re=0.62 x 10⁶.

FIGURE 28.—Schlieren photographs at low Reynolds numbers of models 3 and 6 with roughness added. Knife edge vertical.
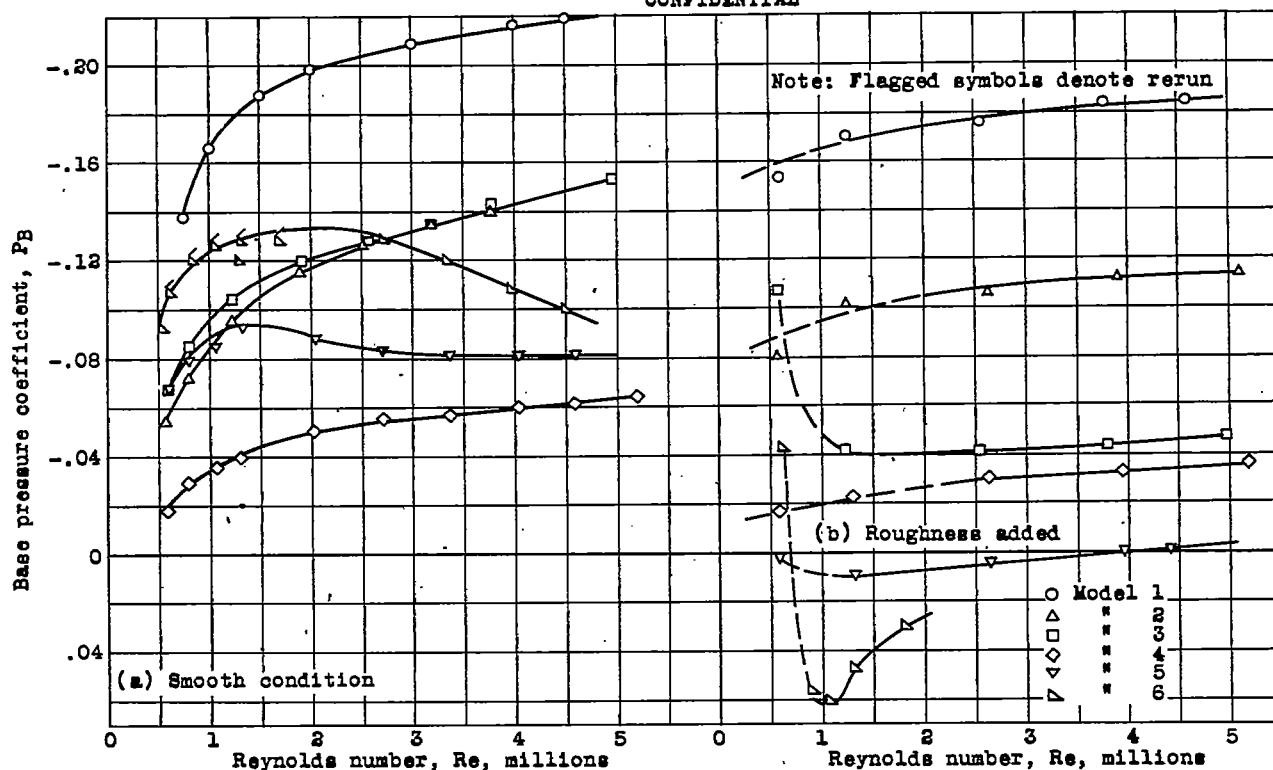
CONFIDENTIAL

CONFIDENTIAL

Figure 29.- Variation of base pressure coefficient with Reynolds number for models 1, 2, 3, 4, 5, and 6 in the smooth condition and with roughness added.
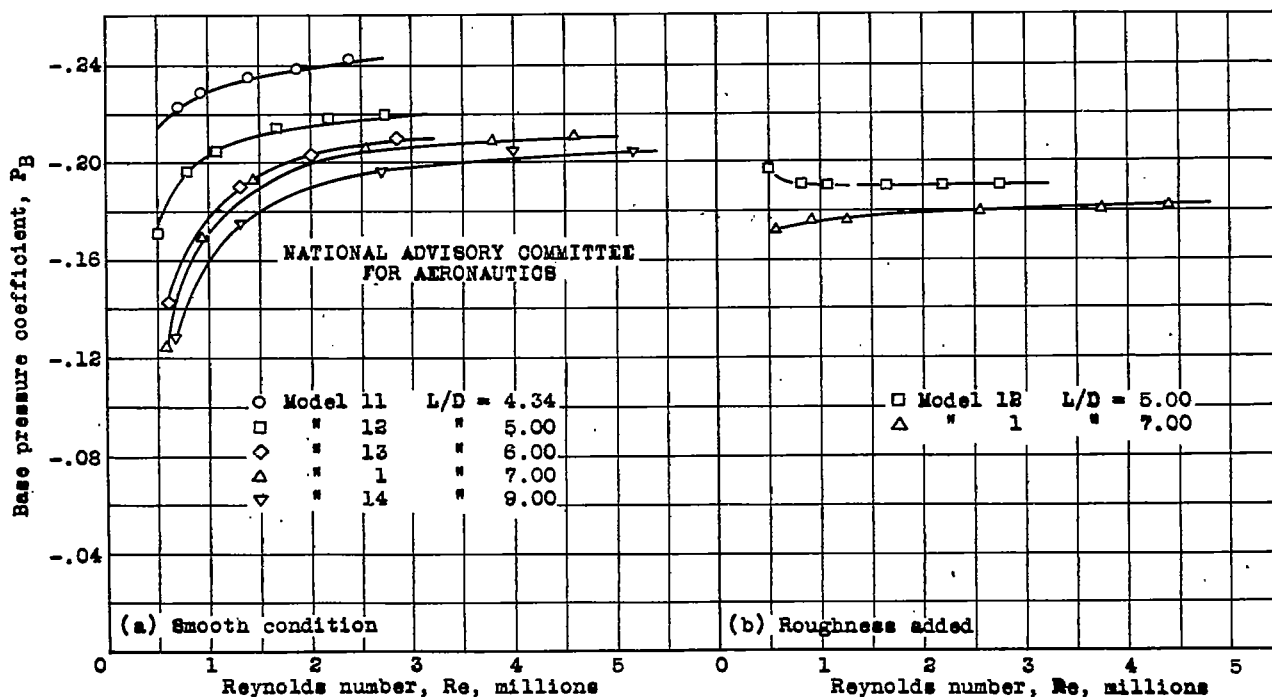

Figure 30.- Variation of base pressure coefficient with Reynolds number for bodies without boat-tailing but with different length-diameter ratios.

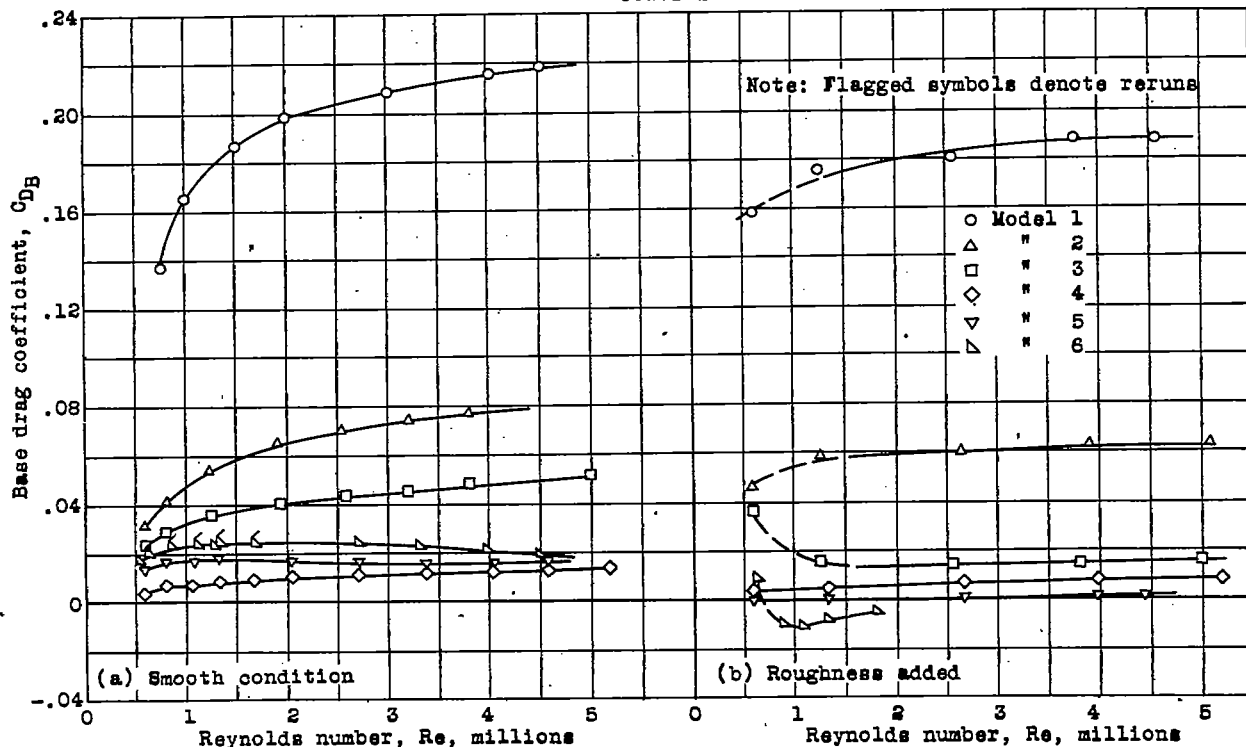CONFIDENTIAL

CONFIDENTIAL

Figure 31.- Variation of base drag coefficient with Reynolds number for models 1, 2, 3, 4, 5 and 6 in smooth condition and with roughness added.
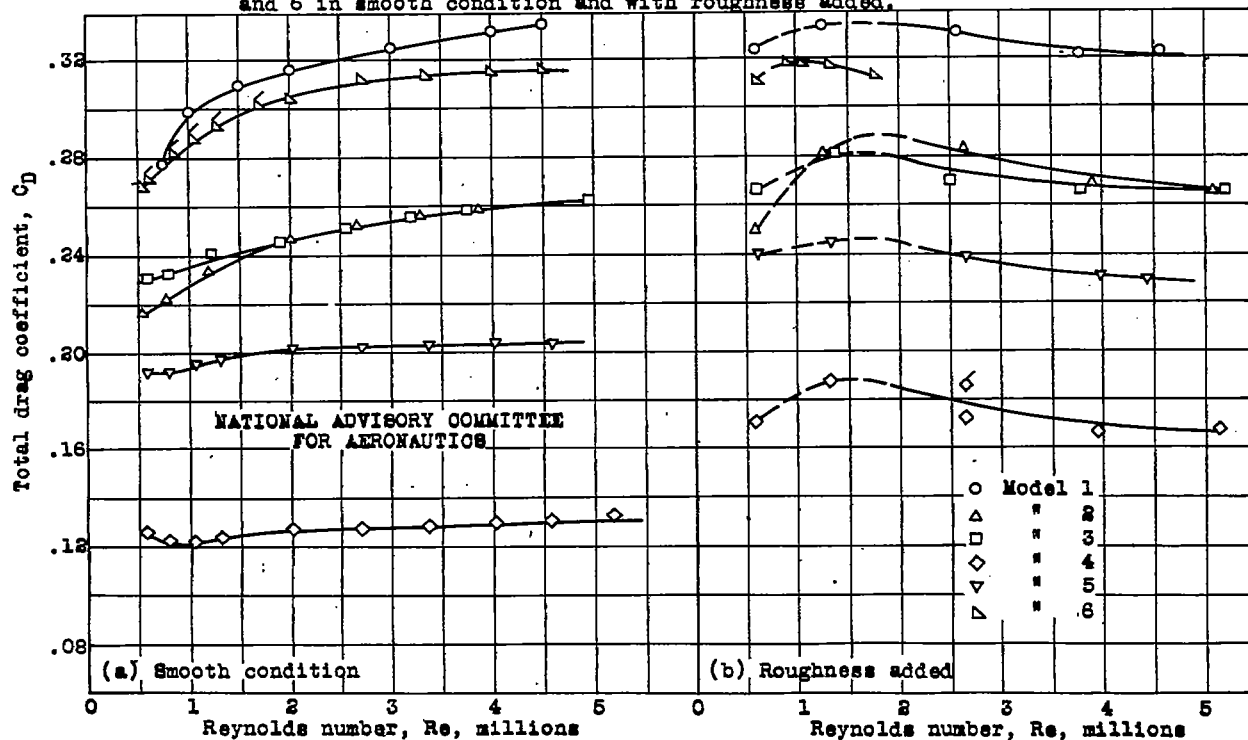

Figure 32.- Variation of total-drag coefficient with Reynolds number for models 1, 2, 3, 4, 5 and 6 in the smooth condition and with roughness added.

CONFIDENTIAL